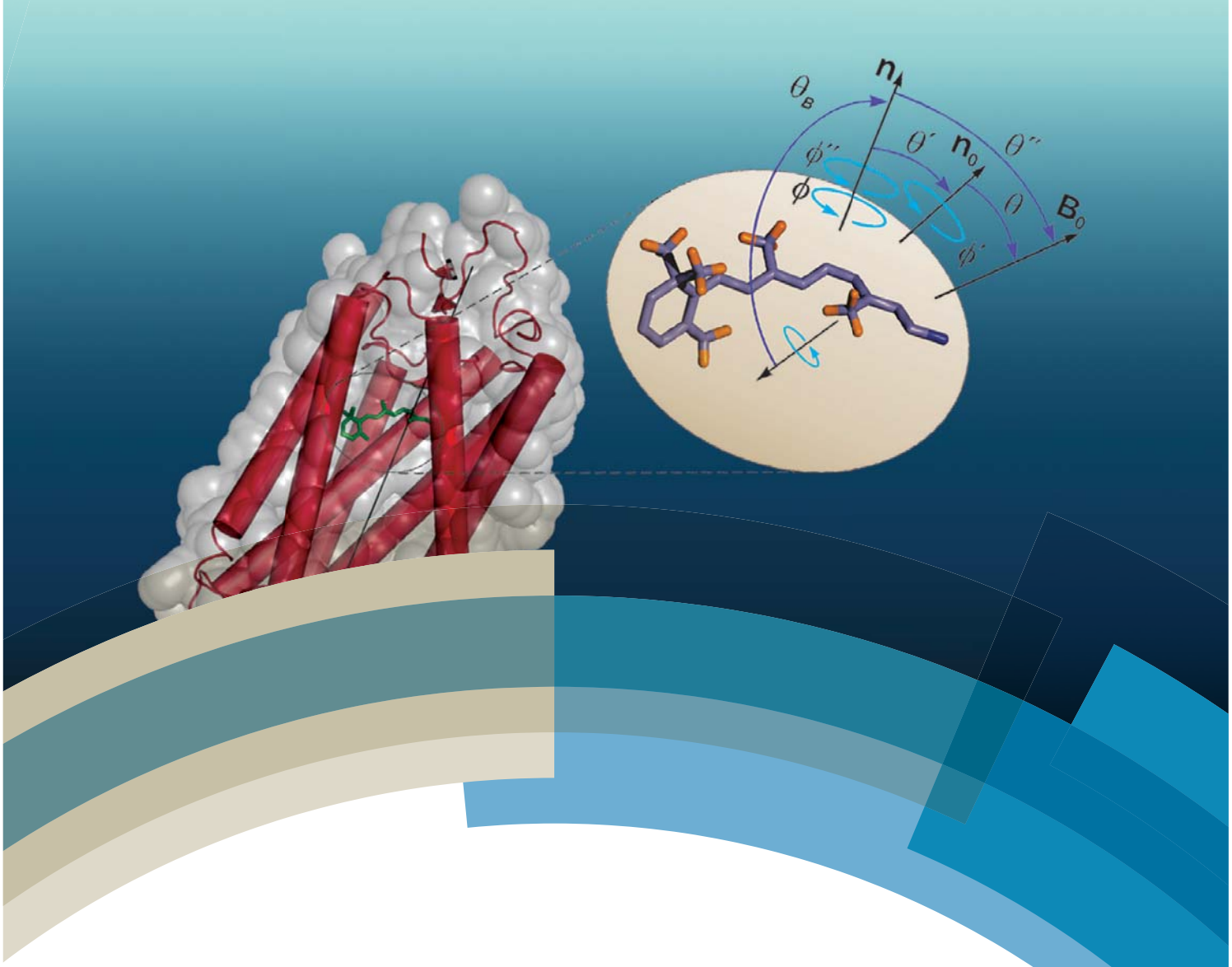

New Developments in NMR

Advances in Biological Solid-State NMR

Proteins and Membrane-Active Peptides

Edited by Frances Separovic and Akira Naito

ROYAL SOCIETY OF CHEMISTRY

CHAPTER 17

Structural Dynamics of Retinal in Rhodopsin Activation Viewed by Solid-State ^{2}H NMR Spectroscopy

MICHAEL F. BROWN*[a,b] AND ANDREY V. STRUTS[a,c]

[a] Department of Chemistry and Biochemistry, University of Arizona, Tucson, AZ 85721, USA; [b] Department of Physics, University of Arizona, Tucson, AZ 85721, USA; [c] Laboratory of Biomolecular NMR, St Petersburg State University, St Petersburg 199034, Russia
*Email: mfbrown@u.arizona.edu

17.1 Introduction

G-protein-coupled receptors (GPCRs) are responsible for signal transduction through cellular membranes[1,2] and have long been a focus of structural studies employing site-directed spin-labelling,[3–6] crystallographic analysis,[7–12] and NMR spectroscopy.[13–22] However, the structures of most GPCRs are currently unknown due to difficulties in their crystallization for X-ray studies and their relatively high molecular weight for solution NMR spectroscopy. In the last few years, X-ray structures of several GPCRs, including rhodopsin,[7–12] the β_1- and β_2-adrenergic receptors,[23–25] the adenosine A_{2A} receptor,[26] and opioid receptors,[27–30] have made possible significant advances in the understanding of their activation mechanisms.[1,2,31,32] Currently, rhodopsin is one of the few GPCRs for which the 3D structures in various functional states have

New Developments in NMR No. 3
Advances in Biological Solid-State NMR: Proteins and Membrane-Active Peptides
Edited by Frances Separovic and Akira Naito

Published by the Royal Society of Chemistry, www.rsc.org

been recently established.[11,12,33–35] Nevertheless, many important details of its structure and activation mechanism remain speculative, and require further investigation by different methods; in particular, the orientation of retinal in the active metarhodopsin II (Meta II) state is not unambiguously determined.[11,12,35]

To understand the activation mechanism of the visual receptor rhodopsin, first, one must characterize the atomistic motions of the ligand and the protein. Next, one must explain how the local changes of the chromophore structure lead to the activating conformational changes of the receptor. A further aspect is that one must establish the role of the membrane lipid bilayer, because it is well known that the lipid environment affects the activation of rhodopsin.[36–39] In the visual process, rhodopsin activation involves the 11-*cis* to 11-*trans* isomerization of retinal due to photon absorption, which leads to movements of the transmembrane helices[3,6] that expose recognition sites on the cytoplasmic loops for the G-protein (transducin). Major local changes include deprotonation of the retinylidene Schiff base that triggers large-scale helical rearrangements in the protein structure, accompanied by disruption of two ionic locks and hydrogen-bonding networks around Glu122 and Asp83 that stabilize the dark-state conformation. Apart from X-ray analysis[7–12] and spin-label ESR studies,[3–6] rhodopsin structure and dynamics have also been studied by vibrational Raman spectroscopy,[40] which gives information about torsional twisting of the retinal chromophore during light activation.

Notably, biophysical and bioorganic investigations of rhodopsin mutants and rhodopsin recombined with various retinal analogues have been extremely useful in identifying key interactions that are implicated in its biological activity.[41–43] Fourier transform infrared studies of desmethyl analogues of retinal bound to rhodopsin have revealed that deletion of the C5-, C9-, or C13-methyl groups of retinal shifts the metarhodopsin equilibrium towards the inactive metarhodopsin I (Meta I) state, thus implicating them in the receptor functioning. Another valuable tool that is complementary to X-ray crystallography is solid-state ^{2}H NMR spectroscopy. One of the advantages of NMR is that membrane proteins are studied in a native-like membrane environment[13,18,44–50] where protein function is preserved.[37,38] Moreover, the structural information obtained from ^{2}H NMR, for example bond orientations, may be more accurate than from X-ray studies. Last, solid-state NMR relaxation experiments[21] reveal dynamical information that cannot be readily obtained with X-ray crystallography or other biophysical methods.[51]

17.2 Order Parameters and Bond Orientations for Membrane Proteins are Determined from Solid-State ^{2}H NMR Spectroscopy

For decades, solid-state ^{2}H NMR spectroscopy has been an irreplaceable tool for studying the structure and molecular motions in polymers and liquid

crystals (including lyotropic liquid crystals such as lipid bilayers). Progress in NMR spectroscopy has made it possible to extend the application of solid-state ^{2}H NMR to the investigation of membrane proteins.[13,44–46,52] Two major difficulties in this area are related to the large linewidth in solid-state ^{2}H NMR spectroscopy: first, this affects the signal intensity for relatively high molecular weight membrane proteins and, second, only a single or at most a few selectively labelled groups can be studied in one experiment. Similar obstacles apply for other solid-state NMR methods that involve nuclei other than deuterium, such as polarization-inversion spin-exchange at the magic angle (PISEMA) and dipolar-assisted rotational resonance (DARR) spectroscopy.[18,53–60] For reviews of solid-state NMR spectroscopy as applied to membrane proteins and peptides, see the Hong *et al.*[56] and McDermott[58] articles.

Figure 17.1 shows theoretical solid-state ^{2}H NMR spectra calculated for a single deuterated group in (a) unoriented or (b, c) aligned systems. The solid-state ^{2}H NMR spectrum is described by the distribution of the spectral intensity as a function of the quadrupolar frequencies, $\nu_Q^{\pm}$, or equivalently the reduced frequencies, $\xi_{\pm}$, for the two single-quantum transitions of the spin $I = 1$ ^{2}H nucleus. For spin $I = 1$ nuclei, the two spectral branches correspond to transitions between energy levels with different projection quantum numbers, $m = -1, 0, +1$, for the spin angular momentum. For an axially symmetric coupling tensor $\xi_{\pm} \equiv \nu_Q^{\pm}/(3/4)\chi$, where χ is the quadrupolar coupling constant (static $\chi = \chi_Q = 170$ kHz; or residual $\chi = \langle\chi_Q\rangle$). Reduced frequencies depend on the angle $\tilde{\theta}$ between the EFG tensor principal z-axis (assuming axial symmetry) and the static external magnetic field $\boldsymbol{B}_0$ according to $\xi_{\pm} = \pm\frac{1}{2}(3\cos^2\tilde{\theta} - 1)$.[61] In the case of random isotropic orientations of molecules in unoriented (non-aligned) samples as in Figure 17.1(a), the angular probability distribution of the nuclear coupling tensor $p(\xi_{\pm})$ and spectral intensities can be expressed as $1/|\cos\tilde{\theta}|$, yielding a so-called powder-type spectrum (or Pake doublet). In the case of a semi-random uniaxial distribution of the coupling tensor, Figure 17.1(b,c), the ^{2}H NMR lineshapes depend on the angle θ of the alignment symmetry axis with respect to the main magnetic field $\boldsymbol{B}_0$, as well as the angle θ_B between the coupling tensor principal symmetry axis and the alignment axis. Consequently, useful structural information, namely bond orientations, is available from ^{2}H NMR spectroscopy of aligned membrane samples.[13,44–46]

Next, in Figure 17.2, we show representative experimental ^{2}H NMR spectra of selectively deuterated methyl groups for retinal bound to the dark-state rhodopsin in non-oriented POPC membranes. The spectral splitting indicates fast spinning of the C5-, C9-, or C13-methyl groups about their C_3 axes with correlation times $<10^{-5}$ s even at low temperatures (down to –150 °C, as shown for the C9-methyl group; Figure 17.2a). The motion-averaged ^{2}H NMR spectral lineshapes involve residual quadrupolar couplings (RQCs) designated by $\langle\chi_Q\rangle$ that correspond directly to the segmental order parameters (Figure 17.2b). The order parameter characterizes the amplitude of the

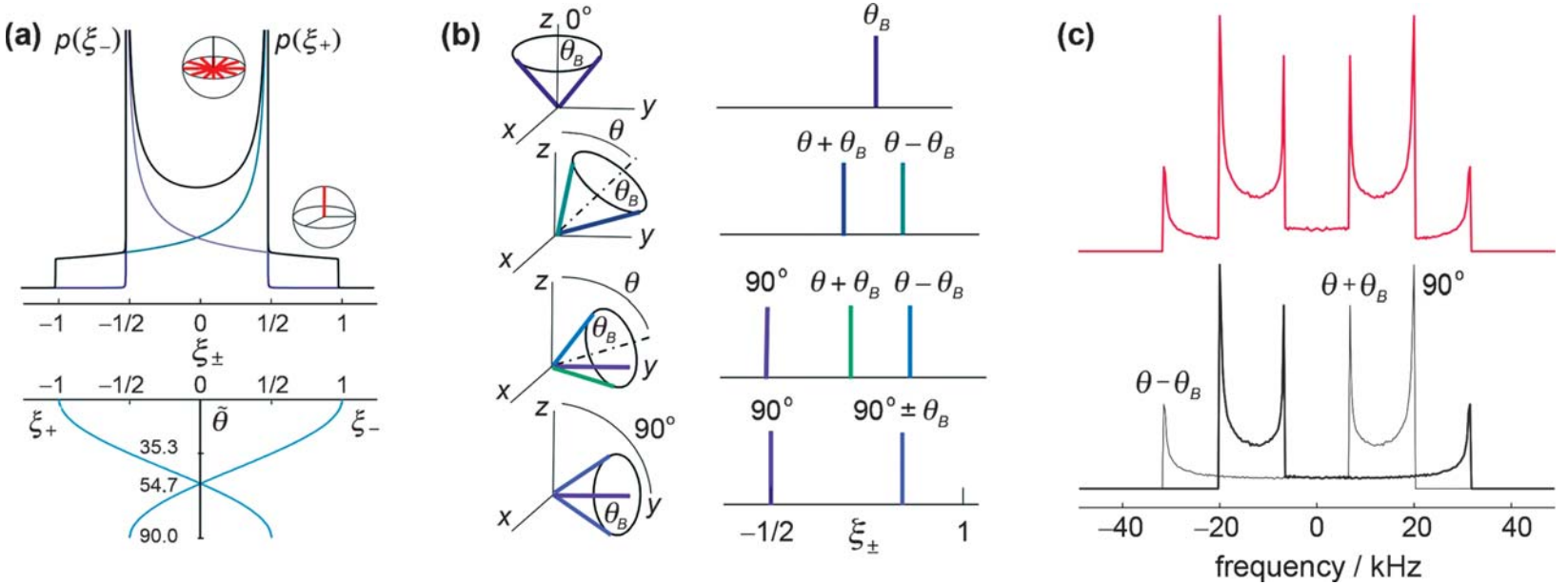

Figure 17.1 In solid-state ^{2}H NMR the spectral frequency distribution is a map of the angular distribution of the electric field gradient (EFG) tensor. (a) For unoriented membrane systems, the principal symmetry axis of the coupling tensor is randomly distributed *versus* the static external magnetic field $\boldsymbol{B}_0$, giving a powder-type spectrum (so-called Pake doublet). The ^{2}H NMR spectrum for the two spectral branches of an $I=1$ spin system is graphed as a function of the reduced frequency $\xi_\pm$ and corresponds to the principal z-axis of the EFG tensor randomly distributed over the surface of a sphere. Note that the probability distribution $p(\xi_\pm)$ scales as $1/|\cos\tilde{\theta}|$, where $\tilde{\theta}$ is the overall angle between the EFG tensor z-axis (assumed axially symmetric) and the $\boldsymbol{B}_0$ field. Weak singularities are evident at $\tilde{\theta}=90^\circ$ (equator) or 35°, with the intensity extending to a minimum at $\tilde{\theta}=0^\circ$ (poles). The spectral centre is where $\tilde{\theta}=54.7^\circ$ (so-called magic angle). Angular dependence of the reduced frequencies is graphed at the *bottom*. (b) Example of semi-random angular distribution of coupling (EFG) tensor principal axis, where θ is the tilt angle of the alignment axis to the main magnetic field $\boldsymbol{B}_0$ and θ_B is the coupling tensor orientation to the alignment axis. For rotating methyl groups, as in the case of retinal bound to rhodopsin, the principal direction of the EFG is the three-fold axis. At *left*, the various orientations giving the intensity maxima for an individual spectral branch of the $I=1$ nucleus are depicted. A static uniaxial distribution is considered where the coupling tensor z-axes are confined to the rim of a cone. Owing to inversion and reflection symmetry, only the distribution for a quarter-sphere is needed. The adjacent schematic (*stick*) spectra are for a single spectral branch. For zero tilt (*top spectrum*), an axially symmetric spectrum is obtained; with increasing tilt angle the spectral features represent the sum and difference of θ and θ_B. At large enough tilt angle, a further weak singularity appears at $\theta=90^\circ$ as for a random distribution. (c) Calculated ^{2}H NMR spectrum for a static uniaxial distribution of methyl groups having three-fold rotation, *e.g.* the case of an aligned membrane protein. The two spectral branches of the $I=1$ ^{2}H nucleus are shown in different colours at the *bottom*, with the resultant spectrum at the *top*. To correspond to the stick spectra in panel (b), the line broadening is intentionally reduced.
(Reproduced from Brown *et al.*,[116] with permission from Elsevier.)

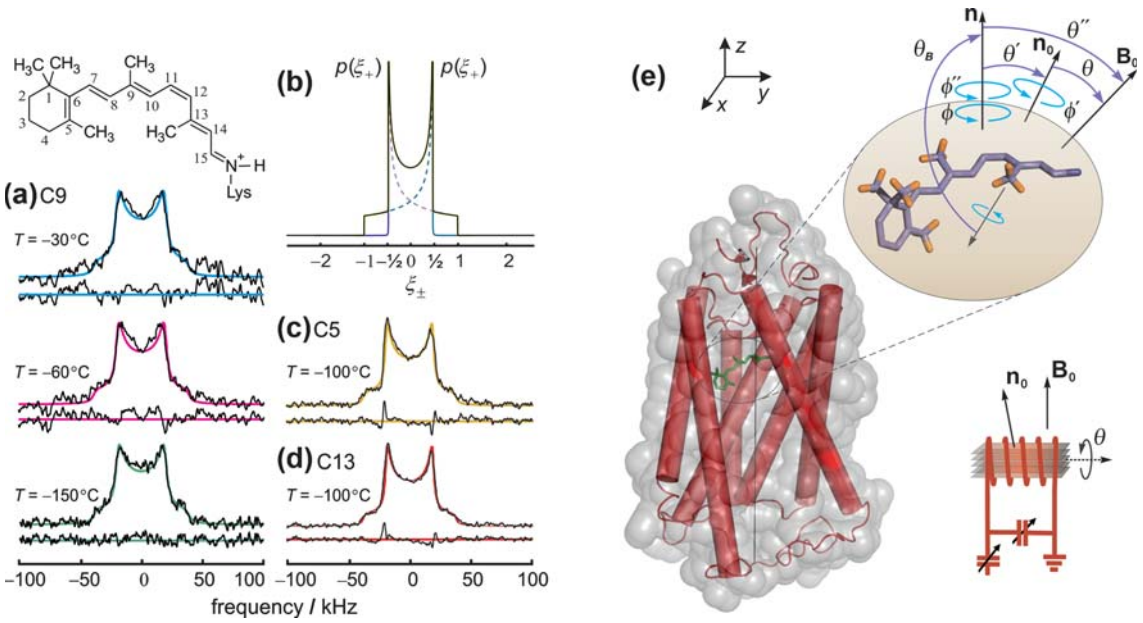

Figure 17.2 Powder-type ^{2}H NMR spectra for membrane-bound rhodopsin with ^{2}H-labelled retinal in the dark state indicate that the methyl groups undergo rapid rotation with large order parameters. (a) Experimental ^{2}H NMR spectra for 11-*Z*-[9-C^{2}H$_3$]-retinylidene rhodopsin, *i.e.* having 11-*cis*-retinal deuterated at the C9-methyl group, in gel-phase POPC membranes (1:50 molar ratio) at different temperatures. (b) Theoretical ^{2}H NMR spectrum for randomly oriented C–C^{2}H$_3$ groups (Pake doublet) undergoing rapid three-fold rotation on the ^{2}H NMR timescale ($<(3\chi_Q/8)^{-1} \approx 10$ μs) plotted on a reduced frequency scale. (c,d) Representative ^{2}H NMR spectra for dark-state 11-*Z*-[5-C^{2}H$_3$]-retinylidene rhodopsin and 11-*Z*-[13-C^{2}H$_3$]-retinylidene rhodopsin, *i.e.* with 11-*cis*-retinal deuterated at the C5-methyl or C13-methyl group, respectively, in POPC membranes (1:50). Theoretical ^{2}H NMR spectra for C–C^{2}H$_3$ groups undergoing axial rotation (*continuous colour lines*) are superimposed on the experimental spectra, with residuals below. (e) Structure and orientation of retinal ligand within the rhodopsin binding cavity are established by solid-state ^{2}H NMR spectroscopy of aligned membranes. For a given methyl group, θ_B is the angle of the C–C^{2}H$_3$ bond axis to the local membrane normal $\boldsymbol{n}$, with static rotational symmetry given by the azimuthal angle ϕ. Alignment disorder is described by the angle θ' of $\boldsymbol{n}$ to the average membrane normal $\boldsymbol{n}_0$ and is also uniaxially distributed as characterized by ϕ'. Next, θ is the tilt angle from $\boldsymbol{n}_0$ to the main magnetic field $\boldsymbol{B}_0$, about which there is cylindrical symmetry. Lastly, θ'' is the angle from $\boldsymbol{n}$ to $\boldsymbol{B}_0$, where ϕ'' is the azimuth. The van der Waals surface of rhodopsin is depicted in *light grey* and the seven transmembrane helices are indicated by *rods*, with the N-terminus at the *top* (extracellular side) and the C-terminus at *bottom* (cytoplasmic side). The schematic depiction of a stack of aligned membranes containing rhodopsin within the radiofrequency coil of the NMR spectrometer shows the geometry relative to the magnetic field.
(Adapted from Struts *et al.*,[20] with permission from Elsevier.)

fluctuations of the coupling tensor, and is defined by $S_{C_3} \equiv \frac{1}{2}\langle 3\cos^2\beta_{IM} - 1\rangle$, where β_{IM} is the angle between the instantaneous and average orientations of the methyl coupling tensor principal symmetry axes. For a rapidly spinning

methyl group, rotation about the three-fold symmetry axis averages the static coupling constant to $\chi_Q^{eff} = \chi_Q(3\cos^2 109.47^\circ - 1)/2 = -\frac{1}{3}\chi_Q = -56.67$ kHz. Off-axial fluctuations additionally reduce the quadrupolar coupling constant, and can be characterized by $S_{C_3} = \langle\chi_Q\rangle/\chi_Q^{eff}$, which is the order parameter of the methyl three-fold (C_3) axis, where the brackets denote a time average. The order parameter for off-axial motion of methyl groups is more accurately determined for a powder-type sample, because fewer fitting parameters are needed than for an oriented sample.

Interestingly, the RQCs and corresponding order parameters for the spinning methyl groups of the retinylidene ligand change little over a broad range of temperature (Figure 17.2c,d). The order parameter S_{C_3} for the off-axial fluctuations of all the methyl groups studied (C5, C9, C13) is approximately the same ($\sim$0.9). The order parameters depend on the mean orientation of the nuclear interaction tensor and are related to the static as well as dynamical disorder. In addition, the intrinsic line broadening is proportional to the transverse (R_2) relaxation rate, which in turn is connected with molecular mobility, whereby narrower NMR lines correspond to faster motion. Evidently, neither the order parameters nor the line broadening show any noticeable changes over the wide temperature range studied (–30 to –150 °C). Further information about dynamics can be obtained from longitudinal (R_{1Z}) and quadrupolar (R_{1Q}) relaxation experiments, as discussed subsequently.

In Figure 17.2(e) we show how the theoretical ^{2}H NMR spectra for the oriented samples can be calculated by assuming a static uniaxial distribution about the average membrane normal.[62] Effectively, we introduce the Jacobian for transforming from the geometric space of the NMR sample to the frequency space of the corresponding NMR spectrum. The theoretical lineshapes depend on the methyl bond orientation θ_B with respect to the membrane normal and on the alignment disorder (mosaic spread), which is assumed to be Gaussian with a standard deviation of σ. The ^{2}H NMR spectra also depend on the tilt angle (orientation of the average membrane normal $\boldsymbol{n}_0$ with respect to the main magnetic field $\boldsymbol{B}_0$). In the gel phase of a lipid bilayer, the membrane proteins do not undergo significant rotational diffusion[63] on the ^{2}H NMR timescale ($\sim$10 μs). The quadrupolar frequencies of the two spectral branches can be expressed as:[61]

$$\nu_Q^{\pm} = \pm \tfrac{3}{4}\chi D_{00}^{(2)}(\Omega_{XL}) \qquad (17.1)$$

where χ denotes the static or residual coupling constant. The symbol $\boldsymbol{D}^{(j)}$ designates the Wigner rotation matrix of rank j, and $\Omega_{XL} = (\tilde{\phi}, \tilde{\theta}, 0)$ are the Euler angles corresponding to overall transformation of the irreducible components of the coupling tensor from its principal axes system (PAS; molecule fixed) to the laboratory coordinate frame, defined by the main magnetic field $\boldsymbol{B}_0$. We assume an axially symmetric coupling tensor, *i.e.* asymmetry parameter $\langle\eta_Q\rangle = 0$ for the case of rotating methyl groups.

Using closure,[61,64] the overall rotational transformation from the PAS to the laboratory frame may then be represented by a series of intermediate frames (Figure 17.2e). The elements of the Wigner rotation matrix can be expressed according to:[61]

$$D_{00}^{(2)}(\Omega_{XL}) = \sum_{m'=-2}^{2} \sum_{m=-2}^{2} D_{0m'}^{(2)}(\Omega_{XN}) D_{m'm}^{(2)}(\Omega_{ND}) D_{m0}^{(2)}(\Omega_{DL}) \tag{17.2}$$

The first set of Euler angles, $\Omega_{XN} \equiv (0, \theta_B, \phi)$, characterizes the orientation of the PAS of the coupling tensor (static or residual; *X* frame in general) relative to the local membrane normal $\boldsymbol{n}$ where θ_B is the bond orientation, and ϕ is the random azimuthal rotation about the local normal (*N* frame); *cf.* Figure 17.2(e). The second transformation $\Omega_{ND} \equiv (0, \theta', \phi')$ treats the disorder of the local membrane normal *versus* the average normal $\boldsymbol{n}_0$ to the membrane surface (*D* frame) in terms of θ' as well as the random azimuth ϕ'. The last transformation describes the tilt of the average membrane normal $\boldsymbol{n}_0$ to the laboratory (*L*) frame (static magnetic field $\boldsymbol{B}_0$). Next, the analytical calculation can be simplified by introducing rank-1 rotation matrix elements (so-called Poor Man's closure),[62] giving the following results:

$$\cos\tilde{\theta} = \cos\theta_B \cos\theta'' - \sin\theta_B \sin\theta'' \cos(\phi + \phi'') \tag{17.3}$$

$$\cos\theta'' = \cos\theta' \cos\theta - \sin\theta' \sin\theta \cos\phi' \tag{17.4}$$

Here $\tilde{\theta}$ is the overall angle of the C–C^{2}H$_3$ bond axis to the magnetic field $\boldsymbol{B}_0$. The angles $\Omega_{NL} \equiv (\phi'', \theta'', 0)$ describe the overall rotation of the local frame to the laboratory frame, where θ'' is the tilt of the local normal, ϕ'' is a phase factor for the two combined transformations,[62] and θ is the tilt angle of the alignment axis to the main magnetic field $\boldsymbol{B}_0$.

After some lengthy calculations,[62] we obtain the following expressions for the two spectral branches of the ^{2}H NMR lineshape:

(i) For $\alpha > \gamma > \delta > \beta$ or $\gamma > \alpha > \beta > \delta$ then:

$$|\, p(\xi_\pm) \,| \propto \frac{1}{|\cos\tilde{\theta}\,|} \int_0^\pi \frac{1}{y} \boldsymbol{K}\left(\frac{x}{y}\right) \exp\left(\frac{-\theta'^2}{2\sigma^2}\right) \sin\theta' d\theta' \tag{17.5}$$

(ii) For $\gamma > \alpha > \delta > \beta$ or $\alpha > \gamma > \beta > \delta$ then:

$$|\, p(\xi_\pm) \,| \propto \frac{1}{|\cos\tilde{\theta}\,|} \int_0^\pi \frac{1}{x} \boldsymbol{K}\left(\frac{y}{x}\right) \exp\left(\frac{-\theta'^2}{2\sigma^2}\right) \sin\theta' d\theta' \tag{17.6}$$

Note that $x \equiv \sqrt{(\gamma - \delta)(\alpha - \beta)}$ and $y \equiv \sqrt{(\alpha - \delta)(\gamma - \beta)}$ in which the cosines of the sum and difference angles are defined as follows: $\alpha \equiv \cos(\tilde{\theta} - \theta_B)$; $\beta \equiv \cos(\tilde{\theta} + \theta_B)$; $\gamma \equiv \cos(\theta - \theta')$; and $\delta \equiv \cos(\theta + \theta')$. In our results, the

kernel $\boldsymbol{K}(k) = F(\pi/2,k)$ represents a complete elliptic integral of the first kind in the normal trigonometric form:

$$\boldsymbol{K}(k) \equiv \int_0^{\pi/2} \frac{dx}{\sqrt{1 - k^2 \sin^2 x}} \tag{17.7}$$

Here the 3D alignment disorder (mosaic spread) is formulated by a Gaussian distribution of the local membrane normal *versus* the average bilayer normal, $p(\theta') = (1/\sigma\sqrt{2\pi}) \exp(-\theta'^2/2\sigma^2)$, where σ is the standard deviation about the mean of $\langle\theta'\rangle = 0$.

The reader can also verify that the above results yield the appropriate limits for large and small alignment disorder. In the limit of very small mosaic spread, the probability distribution $p(\xi_\pm)$ scales as:[45]

$$|\, p(\xi_\pm)\,| = 1/\,|\cos\tilde{\theta}|\,[\cos(\theta + \theta_B) - \cos\tilde{\theta}]^{1/2}[\cos\tilde{\theta} - \cos(\theta - \theta_B)]^{1/2} \tag{17.8}$$

On the other hand, for the limit of very large mosaic spread the results amount to a random (spherical) distribution. The lineshape formula then gives us the well-known Pake doublet:

$$|\, p(\xi_\pm)\,| \propto \frac{1}{|\cos\tilde{\theta}\,|} \propto \frac{1}{\sqrt{1 \pm 2\xi_\pm}} \tag{17.9}$$

Thus the expected results[65,66] are readily obtained.

17.3 Deuterium NMR Spectral Lineshapes Reveal Changes in Structure of Retinal Due to Light Activation of Rhodopsin

Notable applications of site-directed solid-state ^{2}H NMR spectroscopy include membranes containing bacteriorhodopsin,[44–46,62] DNA fibers,[67] and the structure of retinal bound to rhodopsin in the dark and pre-active Meta I state.[20] In our first example, bovine rhodopsin was regenerated with retinal containing selectively deuterated methyl groups at the C5-, C9-, and C13-methyl positions, and recombined with phospholipid bilayers.[13] The membranes were aligned on ultra-thin glass slides, and ^{2}H NMR spectra were measured at different orientations with respect to the main magnetic field $\boldsymbol{B}_0$, as illustrated in Figure 17.2(e). A tilt series of representative ^{2}H NMR spectra for 11-*cis*-retinal bound to dark-state rhodopsin are shown in Figure 17.3(a), together with the root-mean-square deviation (RMSD) of experimental *versus* simulated spectra (Figure 17.3b,c).

Global (simultaneous) fitting of all ^{2}H NMR spectra at different orientations gives well-defined minima, allowing accurate determination of the bond orientation θ_B and mosaic spread σ of the aligned membranes (Figure 17.3b,c). Theoretical ^{2}H NMR spectra are calculated using the above

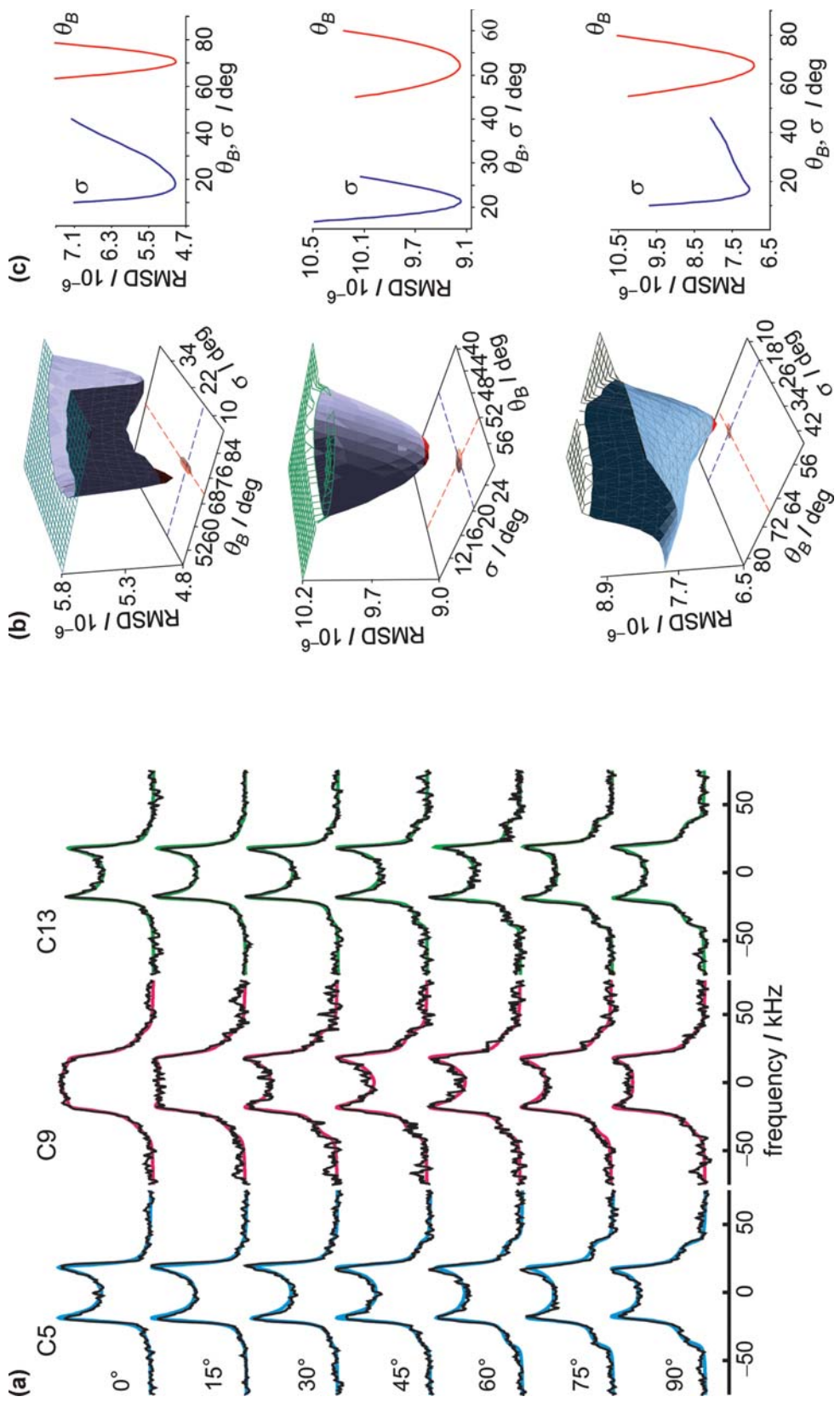
(a)
C5
C9
C13
0°
15°
30°
45°
60°
75°
90°
–50
0
50
frequency / kHz
(b)
RMSD / 10⁻⁶
θB / deg
σ / deg
(c)
σ
θB
θB, σ / deg

formulas (17.5)–(17.7) for a static uniaxial distribution.[62] Alternatively, a Monte Carlo simulation can be employed, where the lineshapes are accumulated numerically by randomly generating the angular variables according to their distribution functions as in Eqns (17.1)–(17.4), together with a Gaussian distribution for the mosaic spread.[62] Both mathematical techniques – the closed-form analysis and Monte Carlo simulation – give essentially identical spectra, thus validating our results. Notably the fitting parameters include the C–C^{2}H$_3$ bond orientation, the mosaic spread, the residual coupling $\langle\chi_Q\rangle$, and the intrinsic line broadening. By comparing the residual coupling $\langle\chi_Q\rangle$ to the effective coupling χ_Q^{eff} we obtain the order parameter for the fluctuations of the C–C^{2}H$_3$ bond axis directly.

In this way, for 11-*cis*-retinal bound to the dark state of rhodopsin, average C–C^{2}H$_3$ bond orientations are obtained of $70 \pm 3^\circ$, $52 \pm 3^\circ$, and $68 \pm 2^\circ$ for the C5-, C9-, and C13-methyl groups, respectively, as shown in Figure 17.3(b). Values for the mosaic spread ($\sigma = 18$–21°) are larger than in previous studies of aligned purple membranes containing bacteriorhodopsin.[45] This finding may be due to the larger molar mass of rhodopsin ($M_r = 40$ kDa) compared to bacteriorhodopsin ($M_r = 26$ kDa), and to the presence of substantial extramembranous domains.[68] It is interesting to note that the ^{2}H NMR bond orientations are in good agreement with independent results from X-ray crystallography.[8,10]

For our next example, experimental solid-state ^{2}H NMR spectra for the retinylidene C5-, C9-, and C13-methyl groups of rhodopsin in bilayers aligned at $\theta = 0^\circ$ are shown in Figures 17.4(a) and 17.4(b) for the dark state and Meta I state, respectively.[47] Further analysis of the retinal conformation entails a simple three-plane model, as illustrated by Figures 17.4(c) and 17.4(d). Deviation of the torsion angles from the ideal *cis* or *trans* configuration is neglected, except for the C6–C7 and C12–C13 bonds, shared by the A–B and B–C pairs of planes, respectively, and the C11=C12 bond.

Figure 17.3 Tilt series of ^{2}H NMR spectra for the 11-*cis*-retinal ligand of rhodopsin in the dark state are explicable by methyl bond orientations and mosaic spread of aligned membranes. (a) ^{2}H NMR spectra for 11-*Z*-[5-C^{2}H$_3$]-retinylidene rhodopsin (*blue*), 11-*Z*-[9-C^{2}H$_3$]-retinylidene rhodopsin (*magenta*), and 11-*Z*-[13-C^{2}H$_3$]-retinylidene rhodopsin (*green*), respectively. Experimental ^{2}H NMR spectra are shown as a function of tilt angle θ between the normal to membrane stack $\boldsymbol{n}_0$ and the magnetic field $\boldsymbol{B}_0$ for rhodopsin/POPC bilayers (1:50) at pH 7 and $T = -150$ °C. Theoretical lineshapes (*continuous colour lines*) assume a static uniaxial distribution of rhodopsin molecules with rotating retinylidene C–C^{2}H$_3$ groups. Global fitting of ^{2}H NMR spectra for 11-*cis*-retinal gives accurate values for methyl bond orientations for the dark state of rhodopsin in aligned membranes. (b) RMSD of calculated *versus* experimental ^{2}H NMR spectra for rhodopsin with retinal deuterated at C5-, C9-, or C13-methyl groups, respectively. (c) Corresponding cross-sections through surfaces at left showing well-defined minima in bond orientation θ_B and mosaic spread σ of aligned membranes.
(Adapted from Struts *et al.*,[20] with permission from Elsevier.)

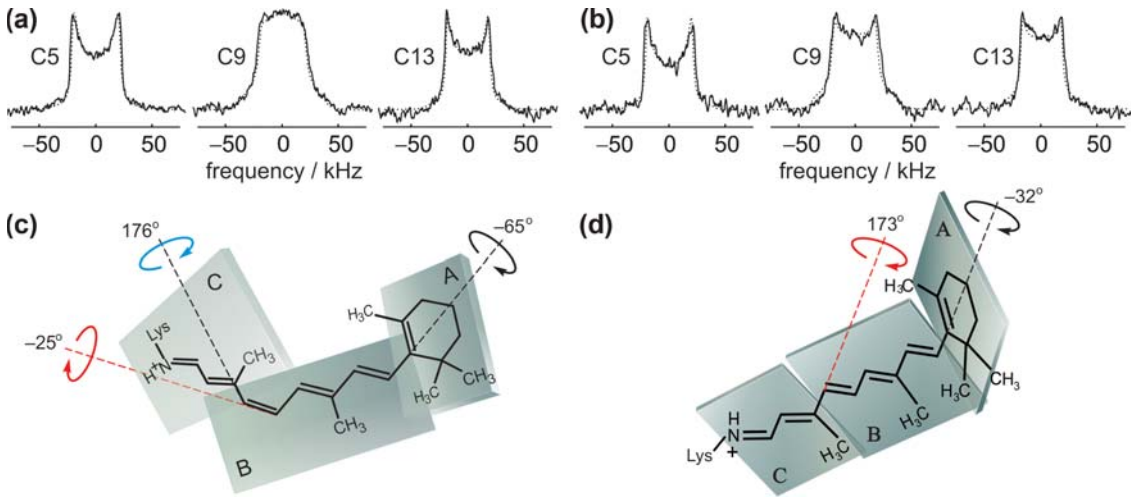

Figure 17.4 Solid-state ^{2}H NMR spectroscopy characterizes the structure of the retinal ligand bound to rhodopsin in aligned membranes. Examples of solid-state ^{2}H NMR spectra are shown for (a) dark and (b) Meta I states of rhodopsin regenerated with 11-*cis*-retinal specifically ^{2}H-labelled at C5-, C9-, or C13-methyl positions in aligned POPC membranes (1:50 molar ratio). The spectra are measured for the parallel orientation ($\theta = 0^\circ$) of the membrane normal to the magnetic field $\boldsymbol{B}_0$ at temperatures of −150 and −100 °C for rhodopsin and Meta I, respectively. (c, d) The solid-state NMR structures proposed for retinal for (c) the dark state of rhodopsin and (d) the Meta I photo-intermediate.

Plane A includes the C5=C6 bond of the β-ionone ring, and planes B and C represent the polyene chain to either side of the C12–C13 bond (see Figure 17.4). Note that each plane is defined by two vectors; thus two angular constraints (degrees of freedom) are needed to specify its spatial orientation. Since the three molecular planes have two common bonds, a total of four independent parameters (degrees of freedom) are needed to define the retinal structure and orientation ($3 \times 2 - 2 = 4$). Together with the C5-, C9-, and C13-methyl group orientations, the electronic transition dipole moment of the retinylidene chromophore from linear dichroism measurements can be introduced as a fourth orientational restraint.[69–72]

According to Figure 17.4, we see that the three ^{2}H-labelled methyl groups lie in the three different planes (A, B, C). This allows the values of the torsion angles $\chi_{i,k}$ between the pairs of planes to be calculated from the individual C–C^{2}H$_3$ bond orientations by the formula:[13]

$$\chi_{i,k} = \cos^{-1}\left(\frac{\cos\theta_i \cos\theta_B^{(i,k)} - \cos\theta_B^{(i)}}{\sin\theta_i \sin\theta_B^{(i,k)}}\right) - \cos^{-1}\left(\frac{\cos\theta_k \cos\theta_B^{(i,k)} - \cos\theta_B^{(k)}}{\sin\theta_k \sin\theta_B^{(i,k)}}\right) \quad (17.10)$$

where $\theta_B^{(i)}$ and $\theta_B^{(k)}$ are the orientations of methyl groups i and k to the local membrane normal $\boldsymbol{n}$, and θ_i and θ_k are angles of the two methyl axes to the common bond between the planes. The angle between the common bond and the local membrane normal is defined as $\theta_B^{(i,k)}$, and is calculated from the C9-methyl orientation, together with the transition dipole moment.

Multiple solutions for the C6–C7 and C12–C13 torsion angles between the A, B, or C planes (and multiple retinal geometries) are obtained for a single set of experimental methyl bond orientations. A total of 64 combinations for the relative orientations of the A, B, and C planes is possible, yielding 128 possible retinal configurations. However, circular dichroism data[73,74] and carbon–carbon distances obtained from solid-state rotational resonance ^{13}C NMR studies[14,17] can be introduced as additional geometrical constraints to find a single physical solution, *e.g.* in analogy to the case of solution NMR spectroscopy.[75]

By this means, Eqn (17.10) is used to obtain the torsion angle of the C12–C13 bond (*i.e.*, the dihedral angle between planes B and C), which is found to be $\chi_{9,13} = +150 \pm 4^\circ$ $(+147 \pm 4^\circ)$. The two values correspond to the C11=C12–C13 bond angle equal to 120° or 130°, respectively. Distortion of the C11=C12–C13 bond angle from ideal orbital geometry (120°) can arise due to interaction of the C13-methyl group with the retinal H10 hydrogen, or it may be induced by the specific configuration of the ligand within the rhodopsin binding pocket. For the β-ionone ring, using positional restraints for the C8-to-C18 and C8-to-C16/C17 distances from solid-state ^{13}C NMR,[14] together with the chirality from circular dichroism studies,[73] the physical solution for the C6–C7 dihedral angle is found to be $\chi_{5,9} = -65 \pm 6^\circ$. The negatively twisted 6-*s-cis* conformation (Figure 17.4c) is most probably due to the non-bonded interactions between the C5-methyl of the β-ionone ring and the H8 hydrogen of the polyene chain.[74,76] The distorted 6-*s-cis* conformation of retinal in rhodopsin agrees with solid-state ^{13}C NMR chemical shift data[77] and differs from the planar 6-*s-trans* conformation seen in bacteriorhodopsin.[45,78] Clearly, the protein environment can modulate the β-ionone ring conformation substantially, which in turn can influence the electronic structure of the polyene[79] and protonation of the retinylidene Schiff base.[80] Notably, the β-ionone ring may undergo torsional fluctuations about the C6–C7 bond, and may be less restricted than the polyene chain, as indicated by molecular dynamics simulations.[81] Mobility of the β-ionone ring within its hydrophobic binding pocket[82] might also explain the fact that it is more difficult to establish a unique conformation for this group using X-ray crystallography.[8,13,14,81,83,84]

Next, to further improve the 11-*cis*-retinylidene ^{2}H NMR structure, it can be inserted into the binding pocket of the X-ray structure of rhodopsin in the dark state (PDB accession code 1U19).[10] However, a simple three-plane model does not fit into the binding pocket, due to multiple steric clashes of retinal with Tyr178 and Cys187 of extracellular loop E2, plus Met207, Tyr268, and Ala292 on helices H5, H6, and H7, respectively. Detailed structural analysis shows that the answer is to allow further twisting of the C11=C12 bond of the polyene chain.[20] Twisting about the C11=C12 bond locates the β-ionone ring within its hydrophobic cavity and is energetically optimal, while maintaining the retinylidene Schiff base near its complex counterion, as in the dark-state rhodopsin structure.[10] The value of the C11=C12 torsion angle can be determined by fitting the C10-to-C20 and C11-to-C20 distances to ^{13}C NMR

rotational resonance data.[17] For the extended three-plane model, the optimum torsion angles for the C11=C12 and C12–C13 bonds are $-25 \pm 10^{\circ}$ and $176 \pm 6^{\circ}$, respectively. Thus, the twist is predominantly localized to the C11=C12 bond. The solid-state NMR structure for retinal is shown in Figure 17.4(c), and it fits perfectly into the retinal binding pocket. Note that the C10-to-C20 and C11-to-C20 distances are relatively insensitive to the C11=C12 torsion angle, giving somewhat large errors. Our proposed torsional twisting of retinal about the C11=C12 double bond agrees with high-resolution X-ray data,[10] and is key to understanding its ultra-fast photoreaction dynamics.[40,85–87] Another interesting aspect is that pre-twisting about the 11-*cis* double bond can govern the chromophore trajectory upon photon absorption.[88] More specifically, we can propose that the binding pocket induces distortion: it prepares the retinal for the isomerization. A negative direction of isomerization about the C11=C12 bond is consistent with hybrid quantum mechanics/molecular mechanics simulations, which indicate that steric interaction of the C13-methyl group with Ala117 hinders rotation toward positive angles.[89] Moreover, the positive helical twist about the C12–C13 bond is in agreement with circular dichroism and bioorganic studies of locked retinoids by Nakanishi and co-workers[74] and with our previous results.[13] Analogous conclusions regarding local twisting about the C11=C12 and C12–C13 bonds have been drawn from combined quantum mechanics/molecular mechanics simulations.[90,91]

The Meta I state has also been cryo-trapped to investigate changes in the retinal conformation and its orientation induced by photon absorption.[20,47] Figure 17.4(b) shows examples of ^{2}H NMR spectra acquired at –100 °C for POPC membranes containing Meta I macroscopically aligned at the $\theta = 0^{\circ}$ tilt angle. The largest differences in the ^{2}H NMR spectra *versus* the dark state are seen for the C9–C^{2}H$_3$ group, with smaller variations for the C5–C^{2}H$_3$ and C13–C^{2}H$_3$ groups. These differences may be pertinent to changes of the bond orientation θ_B and also the mosaic spread σ. The bond orientations of the C5-, C9-, and C13-methyl groups obtained from the ^{2}H NMR spectra in the Meta I state are $\theta_B = 72 \pm 4^{\circ}$, $53 \pm 3^{\circ}$, and $59 \pm 3^{\circ}$, respectively. Owing to the greater alignment disorder (mosaic spread) of Meta I ($\sigma = 22$–25°) compared to the dark state ($\sigma = 18$–21°), the ^{2}H NMR spectra for the C9-methyl are different, whereas the bond orientations are similar. On the other hand, for the C13-methyl group a smaller spectral difference is evident, with a larger change in bond orientation. For Meta I, the ^{2}H NMR spectra indicate that the retinylidene methyl substituents undergo rapid rotation as in the dark state, with order parameters describing off-axial fluctuations of ~ 0.9 within the ligand binding pocket.[20]

Allowable solutions for the C6–C7 torsion angle in Meta I are calculated from the orientational restraints of the methyl groups and the transition dipole moment, together with the ^{13}C NMR distance constraints, yielding $\pm 32 \pm 7^{\circ}$and $\pm 57 \pm 7^{\circ}$ as the results. In addition, two possible values for the C12–C13 dihedral angle are obtained: $\pm 173 \pm 4^{\circ}$. It follows that eight combinations of the dihedral angles corresponding to the retinal structure are allowed. Because electron crystallography does not detect any

rearrangements of the seven transmembrane helices,[92] for retinal the calculated Meta I structures can be further restrained by inserting them into the dark-state rhodopsin structure.[10] Most of the possible retinal structures are eliminated due to the different position of the β-ionone ring in the binding pocket, except for the structure shown in Figure 17.4(d) with $\chi_{5/9} = -32^\circ$ and $\chi_{9/13} = 173^\circ$, and the structure obtained by reflection (mirror symmetry transformation) in a vertical plane with $\chi_{5/9} = 32^\circ$ and $\chi_{9/13} = -173^\circ$. The first structure fits best within the binding pocket, having its only close contact with the functionally important Trp265 side chain. On the other hand, the mirror structure makes close contacts with the side chains of Glu122, Trp265, Tyr268, and Ala292, and thus is less likely.

Figure 17.5 compares the ^{2}H NMR structure of 11-*cis*-retinal in the pre-activated Meta I state (red) *versus* the dark state (green). Evidently, the main changes in the retinal conformation in Meta I encompass rotation of the polyene chain adjacent to the C13-methyl towards the C9-methyl group, accompanied by straightening and elongation of the ligand. The resulting displacement of the β-ionone ring towards helix H5 is also observed by X-ray crystallography and solid-state ^{13}C NMR[11,12,33,93] in different rhodopsin photo-intermediates, and the active Meta II state. Indeed, it plays a crucial role

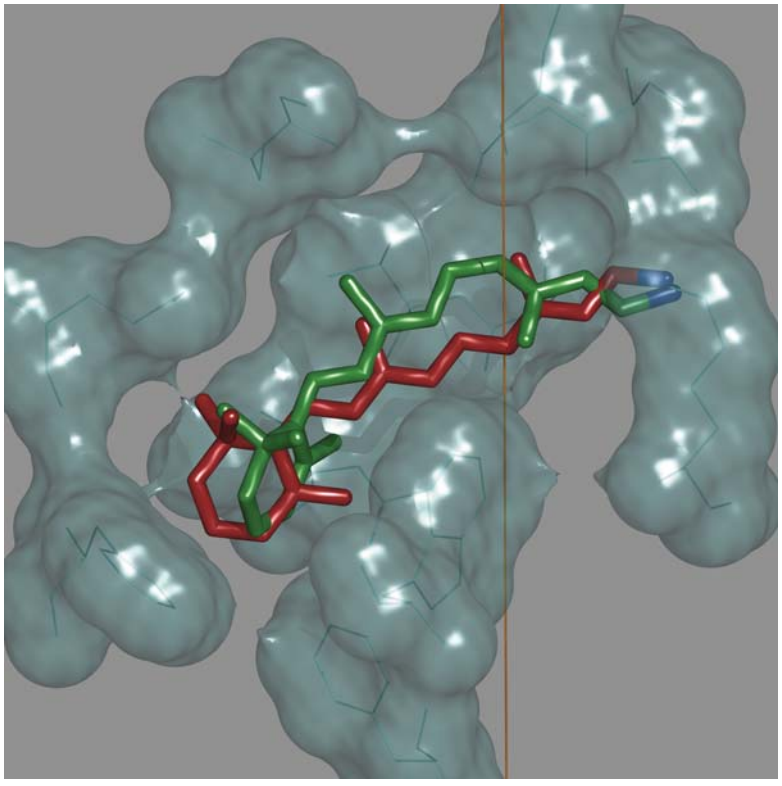

Figure 17.5 Solid-state NMR provides structure of retinal ligand bound to rhodopsin in a natural membrane lipid environment. The vertical direction corresponds to the membrane normal, where the extracellular side is up and cytoplasmic side is down. The ^{2}H NMR structure of 11-*cis*-retinal in the pre-activated Meta I state (*red*) is compared to retinal inserted into the dark state (*green*) X-ray structure (access code 1U19). (Reproduced from Brown *et al.*,[116] with permission from Elsevier.)

in the receptor activation.[94] Rotation of the (proximal) part of the polyene chain containing the C13-methyl group may destabilize the ionic lock involving the protonated Schiff base, and thus facilitate its deprotonation. An apparent steric clash between Trp265 and the retinal may displace the β-ionone ring towards Glu122, whereas Trp265 moves towards helix H5 and the cytoplasmic side of the membrane. These motions are pivotal to the activation process.[95] The β-ionone ring is responsible for disruption of the hydrogen-bonding network around Glu122, which connects helices H3 and H5, and stabilizes the inactive rhodopsin conformation,[94] whereas the displacement of Trp265 underlies the outward activating rotation of the helix H6.[16,18,19,93]

Two additional examples are provided to further highlight the possibilities of solid-state ^{2}H NMR spectroscopy in structural studies of membrane proteins. The next case illustrates the accuracy and sensitivity of the method. In Figure 17.6(a,b) we show experimental and simulated ^{2}H NMR spectra of rhodopsin/POPC recombinant membranes containing 11-*cis*-retinal deuterated at the C5-methyl group of the β-ionone ring. Deuterium NMR spectra for aligned membranes were recorded for a temperature of –60 °C at tilt angles of $\theta = 0^\circ$ or 90° relative to the main magnetic field $\boldsymbol{B}_0$. In Figure 17.6(a) the experimental ^{2}H NMR spectra are superimposed with theoretical fits for a static uniaxial distribution with a bond axis orientation of $\theta_B = 70 \pm 3^\circ$ and a mosaic spread of $\sigma = 21 \pm 2^\circ$. Values for the C5-methyl group were determined from simultaneous non-linear regression fitting of the angular-dependent spectral data.[13] For comparison, Figure 17.6(b) shows theoretical simulations of the same experimental ^{2}H NMR spectra, assuming a C–C^{2}H$_3$ bond orientation of 21° as proposed earlier,[83] together with the above-mentioned value of the mosaic spread. In this case, the experimental line shapes for the C5-methyl group are not reproduced, and thus we conclude that the value of $70 \pm 3^\circ$ is more consistent with the experimental data. Even for relatively large values of the mosaic spread (21° in this example), accurate bond orientations can be determined from the ^{2}H NMR spectra of aligned samples.

The last example in Figure 17.6 illustrates how the experimental ^{2}H NMR spectra of aligned bilayers containing rhodopsin can distinguish between different counterion-switch mechanisms for the protonated Schiff base (PSB) of retinal in the dark state-to-Meta I transition.[96] Figure 17.6(c) shows results for the counterion-switch model, where Glu113 is deprotonated and acts as the counterion to the PSB in the dark state. Proton transfer occurs to Glu113 from Glu181 (tautomerization), which is the new counterion to the PSB upon light absorption. By contrast, in the complex-counterion model shown in Figure 17.6(d), both Glu113 and Glu181 are deprotonated, and the main counterion changes from Glu113 to Glu181 after a photon is absorbed. To decide between these two alternatives, theoretical spectra for the retinal ligand of rhodopsin were calculated numerically for the C5-, C9-, and C13-methyl groups using atomistic molecular dynamics (MD) simulations.[82,96] The continuous colour lines represent theoretical ^{2}H NMR spectra calculated from the methyl group orientational distributions[96] for either the counterion-switch model in Figure 17.6(c) or a complex-counterion

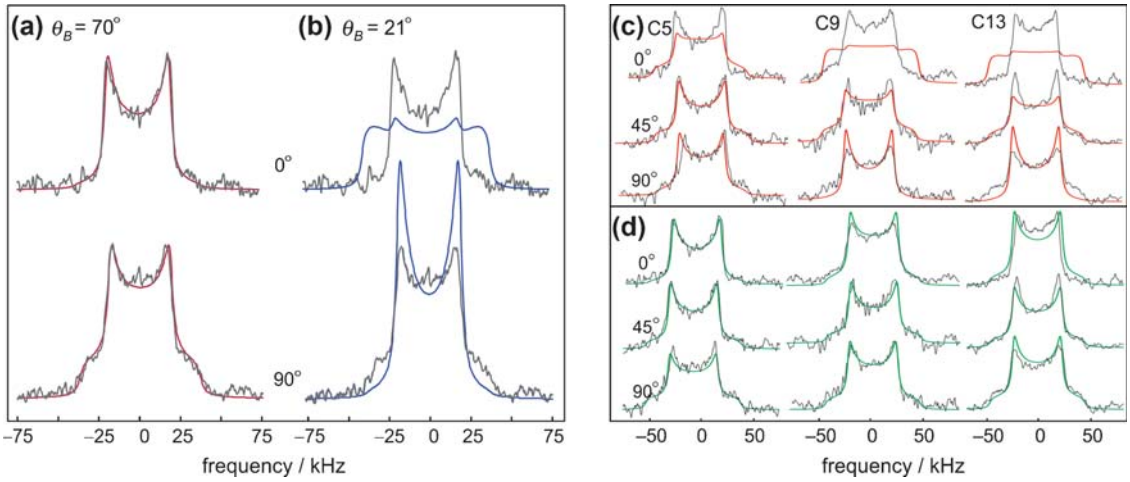

Figure 17.6 Solid-state ^{2}H NMR spectra distinguish various proposed structures for the retinal ligand of dark-state rhodopsin. Experimental ^{2}H NMR spectra are compared to theoretical lineshape simulations.[62] (a) Examples of a C–C^{2}H$_3$ bond orientation[13] of $\theta_B = 70 \pm 3^\circ$ or (b) an alternative[83] of $\theta_B = 21^\circ$ for aligned membranes containing rhodopsin labelled with ^{2}H at the retinal C5-methyl group. Evidently, the former angle is in better agreement with experiment. Results are shown for the $\theta = 0^\circ$ and 90° orientations of the membrane normal to the static $\boldsymbol{B}_0$ magnetic field at –60 °C. Experimental ^{2}H NMR spectra are indicated in *grey* and the *continuous colour lines* depict theoretical spectra for the two proposed[13,83] retinal structures. (c, d) Solid-state ^{2}H NMR spectra for Meta I with retinal ^{2}H-labelled at the C5-, C9-, or C13-methyl groups for $\theta = 0^\circ$, 45°, and 90° tilt angles in aligned membranes at –100 °C.[20] Bond orientation distributions from numerical molecular dynamics (MD) simulations were used to weight the theoretical lineshapes computed for a static uniaxial distribution with a mosaic spread.[62] *Continuous colour lines* based on the MD simulations are shown.[96] Examples are given for (c) counterion-switch model and (d) complex-counterion model for the ionic lock of the protonated Schiff base in the dark-to-Meta I transition. Agreement of the simulated spectra with the experimental data indicates the complex-counterion model applies to rhodopsin.
(Adapted from Salgado *et al.*,[13] and Martínez-Mayorga *et al.*,[96] with permission from American Chemical Society.)

model in Figure 17.6(d). For each methyl group, three representative orientations of $\theta = 0^\circ$, 45°, and 90° for the bilayer normal relative to the magnetic field $\boldsymbol{B}_0$ are shown. Comparing the experimental ^{2}H NMR results to those of the atomistic MD simulations in Figure 17.6 unambiguously favors the complex-counterion switch model.[96]

17.4 Retinal Dynamics within the Binding Cavity of Rhodopsin are Investigated by Solid-State ^{2}H NMR Relaxation Methods

In the case of rhodopsin, ^{2}H NMR relaxation gives a unique, site-directed approach to study the local dynamics of the retinylidene methyl groups

within the ligand-binding pocket.[95] Deuterium spin–lattice relaxation time (T_{1Z}) measurements (decay of Zeeman order) for the C5-, C9-, and C13-methyl groups of retinal have been made for rhodopsin in the dark state, and for the Meta I and Meta II states.[21] In the dark state, the experiments have entailed both non-oriented (powder-type) and oriented membrane samples. Additional experiments in the dark state have determined ^{2}H NMR relaxation times (T_{1Q}) for the decay of quadrupolar order. Measurements were conducted as a function of temperature over a broad interval from -160 to -30 °C. Use of aligned membranes on ultra-thin glass slides with relatively low optical density allowed trapping and characterization of the Meta I and Meta II states of rhodopsin using electronic (optical) spectroscopy.[36,38] By conducting measurements below the melting temperature of the POPC lipid bilayer (-4 °C), the rotational diffusion of the rhodopsin molecules within the membrane was suppressed to reveal the internal dynamics of the receptor-bound ligand.[20] Because the studies were also carried out below the freezing point of water, the interfering signal from the residual ^{2}H nuclei of the water was eliminated.

For the dark state, in Figure 17.7 the experimental temperature dependencies of the deuterium relaxation times for Zeeman (T_{1Z}) and quadrupolar (T_{1Q}) order of the retinal ligand are summarized. First, we note that in Figures 17.7(a,b) the T_{1Z} and T_{1Q} curves with minima at approximately -120 °C are observed for the C5-methyl group. By contrast, the ^{2}H NMR relaxation data indicate that the T_{1Z} and T_{1Q} relaxation times for the C9- and C13-methyl groups of retinal increase monotonically with the temperature (Figures 17.7c,d).[21] The observation of a minimum is important because it corresponds to an optimal matching of the spectral density for the molecular fluctuations to the nuclear Larmor frequency ω_0. It enables an effective correlation time $\tau_c \approx 1/\omega_0$ to be identified for the motions at the corresponding temperature, in accord with NMR relaxation theory.[64] The different T_{1Z} and T_{1Q} minima allow essentially model-free conclusions to be reached about the mobility of the retinylidene methyl groups within the binding cavity of rhodopsin in terms of differences in their correlation times. Shifting the minimum to lower temperature corresponds to faster motions if other conditions (*e.g.* activation energies) are the same. For the C5-methyl group (Figure 17.7a,b), the experimental rotational correlation time exceeds 2 ns at temperatures below approximately -120 °C. However, for the C9-methyl in Figure 17.7(c) and the C13-methyl group in Figure 17.7(d), all motional correlation times are less than $1/\omega_0 \approx 2$ ns down to -160 °C, meaning that the corresponding minima must occur at lower temperatures. Consequently, the ^{2}H NMR relaxation data show significant site-specific differences in the internal mobility of the retinylidene methyl groups within the binding pocket of rhodopsin.

Application of Redfield theory[66] then allows us to establish a connection of experimental relaxation data (Figure 17.7) to the fluctuations of the retinylidene methyl groups within the binding pocket of rhodopsin. Detailed

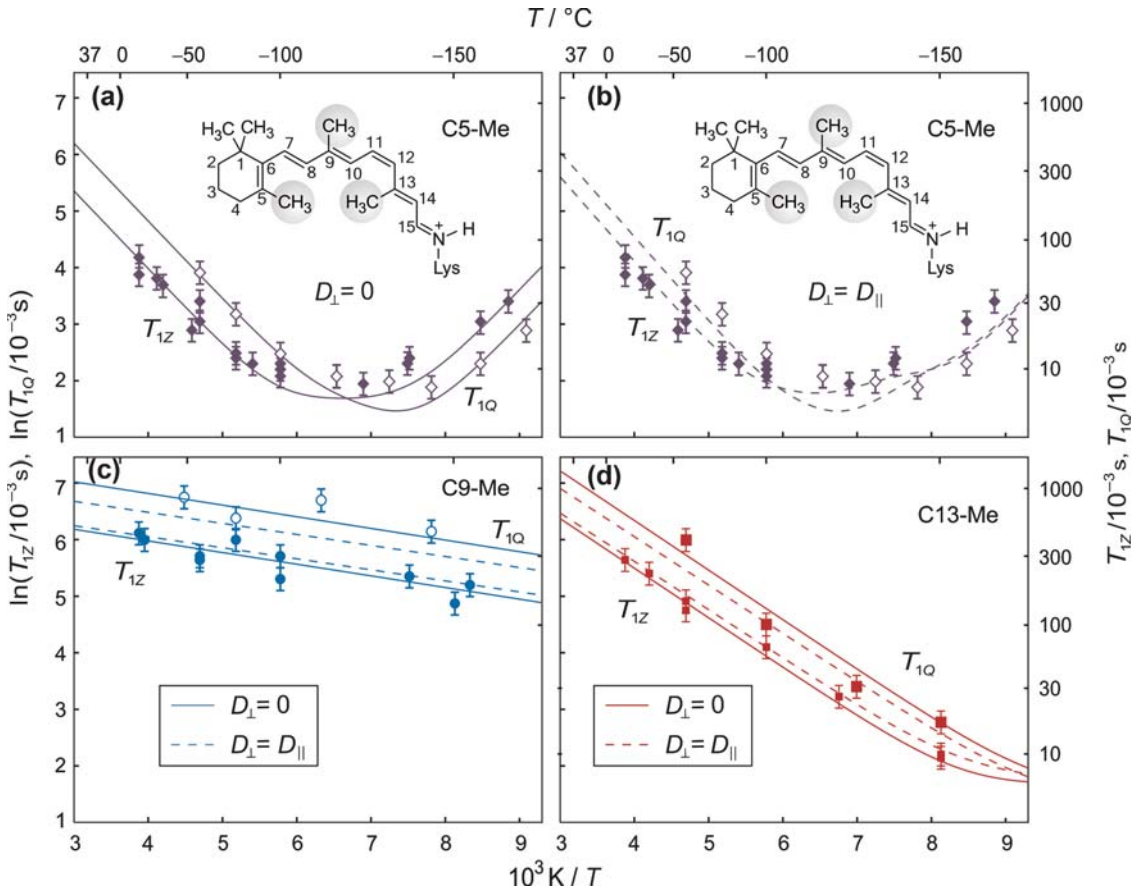

Figure 17.7 Solid-state ^{2}H NMR relaxation uncovers site-specific differences in the mobility of retinal ligand bound to rhodopsin in a membrane environment. Spin–lattice (T_{1Z}) and quadrupolar-order (T_{1Q}) relaxation times are plotted against inverse temperature for rhodopsin in POPC membranes (1:50 molar ratio) in the dark state with retinal ^{2}H-labelled at (a, b) the C5-methyl, (c) the C9-methyl, and (d) the C13-methyl groups. The experimentally determined T_{1Z} and T_{1Q} times were fit using analytical models for molecular dynamics[97] (see text): axial three-fold jump model (rate constant k, *solid lines*) and continuous rotational diffusion model (coefficients $D_\parallel$ and $D_\perp$ with *solid lines* for $D_\perp = 0$ and *dashed lines* for $D_\perp = D_\parallel$).

information about the ligand dynamics is provided, as shown Figure 17.8. The spin–lattice relaxation rates are related to the spectral density (power spectrum) of the thermal fluctuations of the irreducible components of the quadrupolar coupling tensor near the resonance frequency by:[97]

$$R_{1Z} = 1 / T_{1Z} = \tfrac{3}{4}\pi^2\chi_Q^2[J_1(\omega_0) + 4J_2(2\omega_0)] \tag{17.11}$$

and

$$R_{1Q} = 1 / T_{1Q} = \tfrac{9}{4}\pi^2\chi_Q^2 J_1(\omega_0) \tag{17.12}$$

Here χ_Q is the static quadrupolar coupling constant, ω_0 is the resonance (Larmor) frequency, and $J_m(m\omega_0)$ denotes the spectral densities ($m = 1,2$) in

an irreducible representation. In terms of generalized model-free analysis as introduced by Brown,[97] the spectral densities are written as:

$$J_m(\omega) = \sum_{r,q} |D^{(2)}_{0r}(\Omega_{PI})|^2 \left[\left\langle |D^{(2)}_{rq}(\Omega_{IM})|^2 \right\rangle - \left| \left\langle D^{(2)}_{rq}(\Omega_{IM}) \right\rangle \right|^2 \delta_{r0}\delta_{q0} \right] j^{(2)}_{rq}(\omega)\ |D^{(2)}_{qm}(\Omega_{ML})|^2 \tag{17.13}$$

where $\omega = m\omega_0$ and $m = 1, 2$. The quantities in square brackets are the mean-square amplitudes of the fluctuations. Assuming single-exponential relaxation, the corresponding reduced spectral densities for the fluctuations are given by:

$$j^{(2)}_{rq}(\omega) = 2\tau_{rq} / (1 + \omega^2\tau^2_{rq}) \tag{17.14}$$

In Eqn (17.13), $D^{(2)}_{m'm}(\Omega_{ij})$ indicates the Wigner rotation matrix elements with indices m', $m = -2, -1, 0, 1, 2$, and $\Omega_{ij} \equiv (\alpha_{ij}, \beta_{ij}, \gamma_{ij})$ are the Euler angles for rotational transformations between the coordinate systems i and j, where $i,j = P,I,M,D,L$; see Figure 17.8. In our designation, P denotes the principal axis system of the static electric field gradient tensor for a deuterium atom (ordinarily the principal z-axis is parallel to the C–^{2}H bond), I specifies the coordinate system related to the instantaneous orientation of the labelled methyl group, M indicates the system for the average methyl orientation, and L signifies the laboratory axis system (due to the external

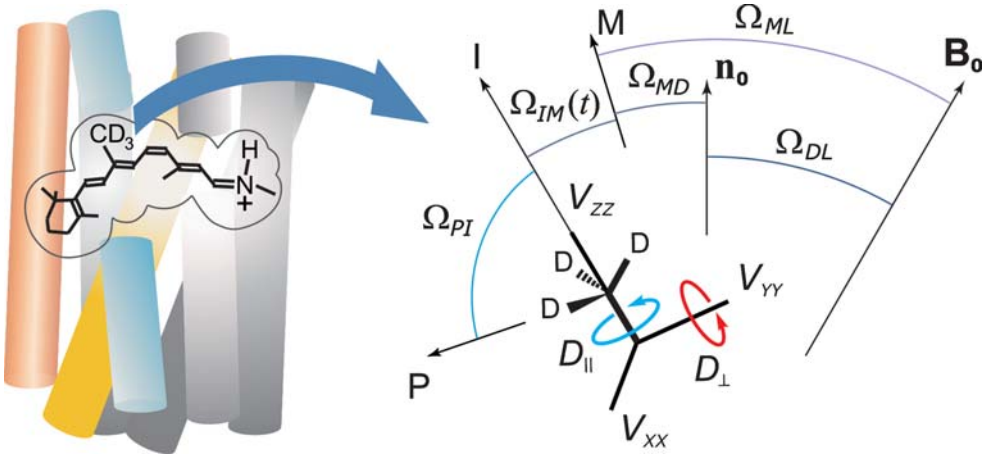

Figure 17.8 Theoretical analysis of the rotational dynamics of retinylidene methyl groups within the ligand pocket of membrane-bound rhodopsin. Euler angles $\Omega_{ij} \equiv (\alpha_{ij}, \beta_{ij}, \gamma_{ij})$ transform among the various coordinate systems $i,j \equiv P,I,M,D,L$. The principal axis system (PAS) of the static EFG tensor of the ^{2}H nucleus is denoted by P (z-axis parallel to C–^{2}H bond), I is the intermediate frame for methyl rotation (z-axis is instantaneous C–C^{2}H$_3$ bond direction), M is the methyl coordinate system (z-axis is average C–C^{2}H$_3$ bond direction), D is the membrane system (z-axis is surface normal $\boldsymbol{n}_0$), and L is the laboratory system (z-axis along external magnetic field $\boldsymbol{B}_0$).[109]

magnetic field $\boldsymbol{B}_0$). According to this notation, for the retinylidene methyl groups $\Omega_{PI} = (0°, 70.5°, 0°)$ and $\Omega_{ML} = (0°, \beta_{ML}, 0°)$. The final coordinate transformation can be further expanded to include the dependence on the membrane orientation relative to the main magnetic field $\boldsymbol{B}_0$ according to the formula:

$$D^{(2)}_{qm}(\Omega_{ML}) = \sum_n D^{(2)}_{qn}(\Omega_{MD}) D^{(2)}_{nm}(\Omega_{DL}) \tag{17.15}$$

where D corresponds to the axis system of the membrane normal. For unoriented (powder-type) samples, averaging over all membrane tilt angles is performed.[97]

Further analysis of the rotational dynamics of the retinylidene methyl groups involves introduction of a specific model for molecular motion (*e.g.* discrete jump, continuous diffusion).[97–102] The choice of a specific motional model enters into the correlation times which appear in the reduced spectral densities (Eqn 17.14). For discussion of motional models, see the work of Meirovitch and Freed.[100–102] In general, NMR relaxation is relatively insensitive to the functional form of the potential,[97,103] although differences between jump and continuous diffusion models are observed for methyl groups in solid amino acids.[104] In our work on rhodopsin, the relaxation was observed to be exponential within experimental error for all temperatures employed.[95] Because deviations from exponential relaxation are not observed, one can adopt the azimuthal average for an N-site jump model, *e.g.* as described by Torchia and Szabo.[99] Alternatively, a continuous diffusion model[105,106] may be employed.[97] If rotation about a single axis is considered, *i.e.* off-axial motion is neglected as in the case of a methyl group, then the result of generalized model-free analysis[97] (Eqn 17.13) simplifies to:[107]

$$J_m(\omega) = \sum_{r \neq 0} |D^{(2)}_{0r}(\Omega_{PI})|^2 j^{(2)}_r(\omega) |D^{(2)}_{rm}(\Omega_{IL})|^2 \tag{17.16}$$

where[97,99]

$$1/\tau_{rq} \rightarrow 1/\tau_r = \begin{cases} 4k \sin^2(\pi r/N) & (N\text{-site jump with azimuthal averaging}) \\ r^2 D_{\|} & (\text{axial diffusion}) \end{cases} \tag{17.17}$$

Here k is the rate constant for discrete N-fold axial nearest-neighbour jumps, and $D_{\|}$ is the diffusion constant for continuous axial rotation.

The above results can also encompass both axial and off-axial motions, as included in Eqn (17.13) for the generalized model-free approach.[97] For simplicity, here we adopt[98] a model of continuous rotation diffusion in a potential of mean torque,[97,108] as originally introduced by Pier Luigi Nordio.[105,106] The rotational correlation times are then given by:

$$\frac{1}{\tau_{rq}} = \frac{\mu_{rq}}{\left\langle |D^{(2)}_{rq}(\Omega_{IM})|^2 \right\rangle - \left| \left\langle D^{(2)}_{rq}(\Omega_{IM}) \right\rangle \right|^2 \delta_{r0}\delta_{q0}} D_{\perp} + (D_{\|} - D_{\perp}) r^2 \tag{17.18}$$

where $D_{\|}$ and $D_{\perp}$ are the rotational diffusion coefficients for rotation of the labelled methyl group about its three-fold axis and for the off-axial fluctuations, respectively. In addition, μ_{qn} and $\langle |D_{qn}^{(2)}(\Omega_{MD})|^2 \rangle$ are the moments and mean-squared moduli of the Wigner rotation matrix elements for a generalized potential of mean torque.[98,109] Their values are tabulated in terms of the order parameters in Trouard *et al.*[98] In the limit of a strong-collisional approximation, the methyl orientation is assumed to change randomly by any amount, due to rapid variations in the torque acting upon the segment. The orientation after a collision is independent of that before a collision, and the time taken for a transition is negligible. Hence, the orientation after a collision is given by the orientational probability distribution, leading to:[97]

$$1 / \tau_{rq} \rightarrow 1 / \tau_r = 6D_{\perp} + (D_{\|} - D_{\perp})r^2 \tag{17.19}$$

Lastly, if we assume that the correlation times follow an Arrhenius activation law, then the temperature dependence for either the N-site jump[99] or continuous diffusion[97] model is a simple exponential. For the $N = 3$-site jump model, $1/\tau_{rq} \rightarrow 1/\tau_r = 3k$, where:

$$k = k_0 \exp(-E_a / RT) \tag{17.20}$$

in which k_0 is the jump rate in the absence of the potential and E_a is the potential barrier height or activation energy. For a continuous rotational diffusion model, $1/\tau_r$ is related to the principal values of the rotational diffusion tensor (Eqn 17.18) by:

$$D_{\|} = D_{0\|} \exp(-E_{a\|} / RT) \tag{17.21}$$

and

$$D_{\perp} = D_{0\perp} \exp(-E_{a\perp} / RT) \tag{17.22}$$

The pre-exponential factors ($D_{0\|}$, $D_{0\perp}$) represent the maximum diffusion constants when $E_a \ll RT$, *i.e.* at infinite temperature. Here the values of k_0 (or D_0) and E_a describe the local protein packing influences on retinal within the rhodopsin binding cavity.

In our work, both the three-fold jump model of axial methyl rotations[99] and the continuous diffusion model[97] have been employed to fit the T_{1Z} and T_{1Q} temperature dependencies for retinal bound to rhodopsin[21] in the dark state. In principle, T_{1Z} measurements at different orientations for aligned samples, or at different frequencies for the powder-type samples, allow one to distinguish between the different types of motion. The axial jump model predicts a 20% difference in the methyl relaxation depending on orientation, whereas for an axial free-diffusion model the methyl relaxation is angle independent.[99] For powder-type samples, due to the relatively low signal-to-noise ratio, T_{1Z} is typically measured for the $\beta_{ML} = 90^{\circ}$ orientation of the methyl axis to the main magnetic field $\boldsymbol{B}_0$ (close to the $\theta = 90^{\circ}$ peaks in the

^{2}H NMR spectra). By contrast, aligned samples are often studied with the average membrane normal parallel to the magnetic field ($\beta_{DL} = 0^\circ$). Here, the β_{ML} angle is determined by the orientation of the methyl group in the sample with respect to the membrane normal (director). Differences in the relaxation times for different orientations were found to be undetectable within the error of the measurements, consistent with a diffusion model for the methyl rotational dynamics.

On the other hand, the error of the T_{1Z} measurements (10–20%) is also comparable with the predicted relaxation anisotropy for a jump model, so that firm conclusions cannot be reached regarding the motional mechanism. For the diffusion model, the $\eta_D = D_\parallel / D_\perp$ ratio could not be determined unambiguously based only on the T_{1Z} relaxation times. The T_{1Z} temperature dependencies could be fitted with η_D values of either 1 or ∞ (axial diffusion). The differences in E_a do not exceed 20%, depending on whether only axial diffusion ($D_\perp = 0$) is considered or off-axial motions ($D_\perp = D_\parallel$) are also considered. However, simultaneous fitting of the T_{1Z} and T_{1Q} temperature dependencies for two continuous diffusion models shows that $\eta_D = \infty$ gives good results (Figure 17.7; solid lines), while the fit with $\eta_D = 1$ (Figure 17.7; dashed lines) cannot be regarded as satisfactory, indicating that $\eta_D \gg 1$. This result is probably to be expected, considering the restricted off-axial fluctuations of the retinal methyl groups. The value of ~ 0.9 for the S_{C_3} order parameter corresponds to an amplitude of $\beta_{IM} \approx 15^\circ$ for the off-axial fluctuations of the methyl groups of retinal within the binding pocket of rhodopsin. This motion includes libration of the methyl groups with respect to the unsaturated polyene, as well as any reorientations of the polyene chain and β-ionone ring within the binding cavity. Evidently, the inertial tensors for off-axial fluctuations are larger than for methyl spinning. Correlation times are obtained in the range of 2–12 ps at 30°C and 3–45 ps at –60°C, depending on the methyl position, which are in the range expected for methyl rotation.[21]

At temperatures above the T_{1Z} minimum, the slopes of the T_{1Z} and T_{1Q} dependencies (Figure 17.7) correspond to the activation energy for methyl rotation, and are related to the heights of the rotational potential barriers.[21] The ^{2}H NMR relaxation studies show large site-specific differences in the dynamics, as manifested by both the pre-exponential factor and activation barriers for the retinal motions. To a certain degree, this is surprising considering that the S_{C_3} order parameters and the amplitudes of the off-axial fluctuations for the C5-, C9-, and C13-methyl groups are approximately the same. Values of the experimentally determined activation energies range from 2 to 15 kJ mol^{-1}, depending on the methyl position, and are essentially independent of whether a three-fold jump or a continuous diffusion model is considered. The highest activation energy is for the C5-methyl, with $E_a \approx 15$ kJ mol^{-1}, as is typical of methyl groups in organic solids. The high activation energy for the C5-methyl group is consistent with a 6-*s*-*cis* conformation of the β-ionone ring, which is in agreement with solid-state ^{13}C NMR chemical shift data[77] as discussed above. The surprisingly low

activation energy for the C9-methyl group in the dark state can be explained by compensation of intra-retinal 1–6 interactions with hydrogens H7 and H11 (Figure 17.7c), because as shown by Struts *et al.*[21] the corresponding rotational potentials are displaced *versus* one another by about 180°. The higher activation energy for the C13-methyl groups is evidently due to intra-retinal 1–7 interactions with the H10 hydrogen atom. Contributions due to interactions with the side chains in the binding pocket of rhodopsin in the dark state are secondary, on account of the large distances from the retinylidene methyl groups (>4 Å), *e.g.* see Figure 17.5. Interestingly, the ^{2}H NMR relaxation data imply that the C5-methyl is the least mobile at low temperatures, despite the fact that the β-ionone ring may have multiple conformations that interconvert within the hydrophobic binding pocket on a longer timescale.[81]

After isomerization, notable changes in the molecular dynamics of retinal are evident in the Meta I and Meta II states, as shown in Figure 17.9. The largest light-induced difference involves the C9-methyl group, which is known to be crucial to the process of rhodopsin activation.[110] The E_a barrier for the C9-methyl group is increased approximately two-fold upon isomerization. At the same time, the E_a value for the C13-methyl group is reduced in the Meta I state, and the values of T_{1Z} for the C9- and C13-methyl groups become nearly the same. This seems logical, considering the all-*trans* conformation of the retinal after isomerization, where the C13- and C9-methyl groups may have similar rotational potentials (Figure 17.9). A reduction of the C13-methyl activation energy in Meta I can be explained, analogously to the C9-methyl group in the dark state, in terms of anti-phase potentials for the intra-retinal C13-to-H11 and C13-to-H15 1–6 interactions.[21] The more restricted mobility for the C9-methyl group upon isomerization may indicate a more crowded environment, *e.g.* smaller C9-to-H7 and C9-to-H11 distances in all-*trans*-retinal with respect to 11-*cis*-retinal, or non-bonded interactions with surrounding side chains in the binding pocket (Tyr268 or Thr118). For the C5-methyl group in Meta I, other differences are seen in the temperature dependence of the T_{1Z} relaxation times (Figure 17.9), with possible evidence for two individual minima. In this case, fitting of the experimental relaxation data requires two components with different activation energies E_a and pre-exponential factors (k_0 and D_0). The two components may correspond to different types of motion of the methyl groups (rotation and reorientation), or alternatively two 6-*s*-*cis* conformers of the retinal may be present.[81]

In the transition from the Meta I to the Meta II state, further changes are observed in the dynamics of the retinal. Theoretical fits in Figure 17.9 indicate the activation energy E_a and diffusion constants D_0 increase slightly for the C9-methyl group but decrease for the C13-methyl group.[21] The Meta II state is of particular interest because it is the activated receptor conformation.[111] Minor differences in the rotational dynamics and the activation energies of the C9- and C13-methyl groups in Meta II most likely can be attributed to interactions with amino acid side chains forming the

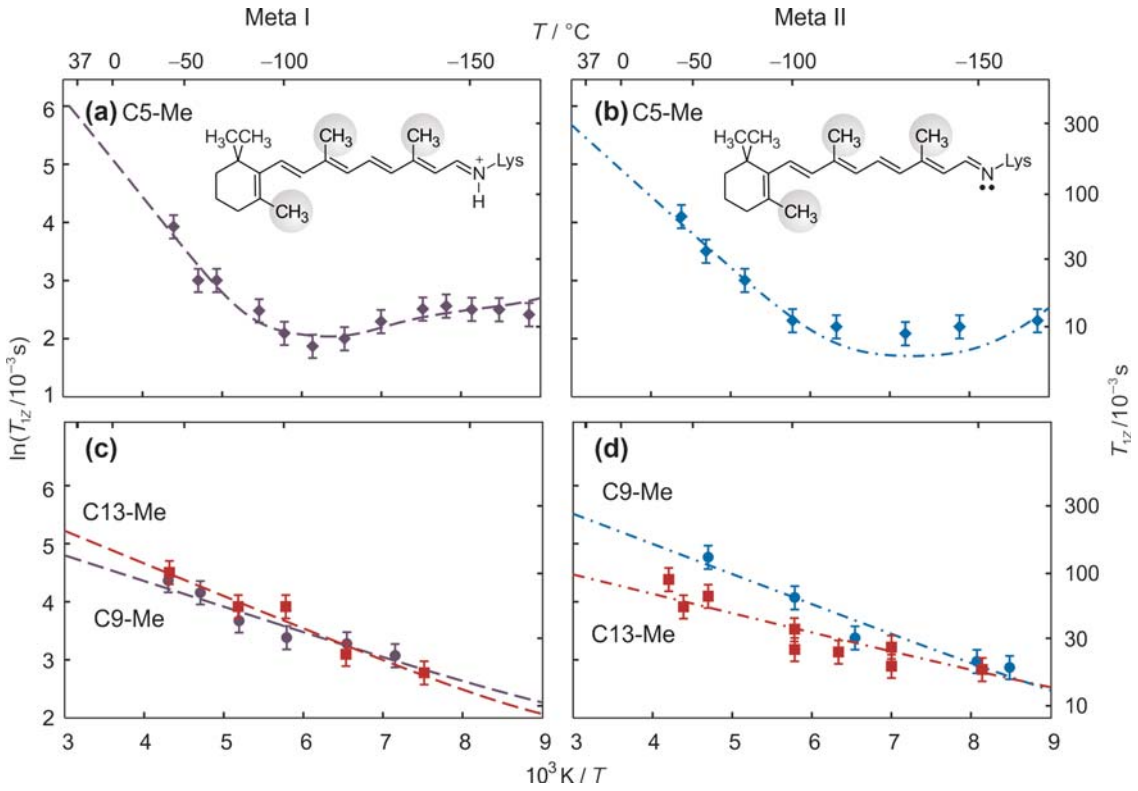

Figure 17.9 Solid-state ^{2}H NMR relaxation illuminates how the dynamics of the retinylidene methyl groups vary upon light activation of rhodopsin in membranes. Spin–lattice relaxation times (T_{1Z}) are plotted against inverse temperature for rhodopsin in POPC membranes (1:50 molar ratio) with retinal ^{2}H-labelled at the C5-, C9-, or C13-methyl groups in (a, c) the Meta I and (b, d) the Meta II states, respectively. The relaxation data are fit with an axial three-fold jump model (rate constant k) as well as with a diffusion model (axial coefficient $D_\parallel$ with $D_\perp = 0$). For the C5-methyl group in Meta I, either different rotational diffusion constants were assumed ($D_\parallel \neq D_\perp$, not shown) or different conformers.[95] Following 11-*cis* to 11-*trans* isomerization, a reduction occurs from three distinct methyl environments in the dark state to roughly two environments in Meta I and Meta II, suggesting a more planar retinal conformation.
(Adapted from Brown and Struts,[117] with permission from Springer.)

chromophore binding pocket. Yet the relatively low activation energies of the C9- and C13-methyl groups in the Meta II state indicate the absence of steric clashes of these groups with residues in the binding cleft. Surprisingly, the C13-methyl has a lower activation energy E_a for axial rotation than the C9-methyl group, although rotation of the C13-methyl group due to retinal isomerization should bring it very close to the β4 strand of extracellular loop E2. A possible explanation for the absence of interactions between the C13-methyl and Cys187 on the β4 strand is that a displacement of the retinal polyene chain away from the E2 loop occurs, due to the polyene chain straightening. This is in agreement with ^{13}C NMR distance measurements[54] and the X-ray structures reported for the putative Meta II state.[11,12,35] According to our relaxation data, such a displacement already takes place

in the Meta I state. Thus, if a steric clash occurs between the C13-methyl and the β4 strand, it is transient. Interestingly, the overall behavior of the T_{1Z} relaxation times for the C5-methyl group in the dark, Meta I, and Meta II states is quite similar (the differences in E_a hardly exceed 20% for a given model of the rotational dynamics, *e.g.* see Figures 17.7 and 17.9). Hence, one can conclude that the conformation and the environment of the β-ionone ring remain similar after rhodopsin activation.[21] A similar conclusion has been reached based on ^{13}C NMR chemical shift data.[16]

17.5 Solid-State ^2H NMR Spectroscopy Illuminates the Activation Mechanism of Rhodopsin in a Membrane Environment

Current knowledge of the rhodopsin activation process entails a sequence of transformations among various states and substates (including photorhodopsin, bathorhodopsin, lumirhodopsin, Meta I, Meta II_a, Meta II_b, and Meta II_bH^+), where Meta II_b and Meta II_bH^+ are considered as the active conformational substates. The substates from Meta I to Meta II_bH^+ are in a quasi-thermodynamic equilibrium after the last stage of the activation is reached. It has been suggested that an ensemble of substates occurs due to the entropy gain produced by release of the inhibitory retinal lock.[95] The picture of rhodopsin activation[21,95] shown in Figure 17.10 is revealed by combining data for the ^2H NMR retinal structure and dynamics in different states with the results of other structural and biophysical studies.[6,11,12,18,33,74,93,94,112]

First, photo-isomerization of retinal leads to the rotation of the C13-methyl group and the adjacent part of the retinal polyene chain towards the β4 strand of the extracellular loop E2.[20,33] In addition, the polyene chain of the retinal straightens and elongates due to the 11-*cis* to 11-*trans* isomerization.[11,20] Straightening of the polyene chain leads to a steric clash with Trp265, accompanied by its displacement towards the cytoplasmic end of the protein, and towards helix H5 (see Figure 17.10).[11,18–20] The displacement of Trp265 of helix H6 may enable outward rotation of helix H6.[18–20] The retinal elongation also results in a translation of the β-ionone ring towards the H5 helix. Rotation of the retinal polyene chain at the Schiff base end of the ligand destabilizes the hydrogen bonding networks connecting the E2 loop, helices H1–H3, H6, H7, and retinal in the inactive state.[8,10,11,112] Additionally, the ionic lock of the protonated Schiff base with its counterion may be destabilized by the 11-*cis*- to all-*trans*-retinal isomerization, which changes the pK_a of the protonated Schiff base.[112] As a result, the hydrogen-bonding network rearranges[11] and the Schiff base deprotonates, breaking the ionic lock and enabling a rearrangement of the helical bundle. Displacement of the β-ionone ring (whose C5-methyl group is in the vicinity of Glu122) towards helix H5 is apparently coupled to rearrangement of another hydrogen-bonding network between Glu122 on H3 and His211 on H5,[11,20,94] which initially stabilizes the inactive conformation. The rearrangement of a

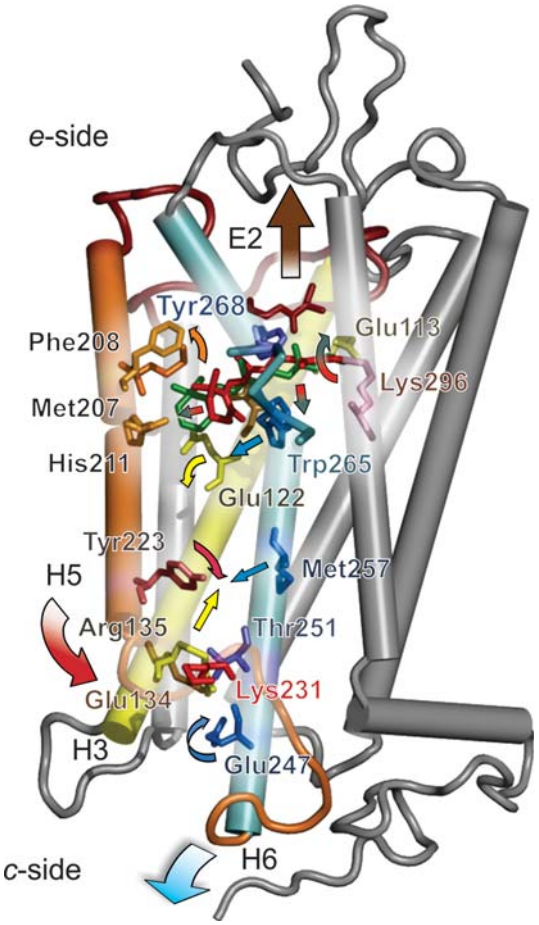

Figure 17.10 Local retinal dynamics underlie large-scale protein rearrangements leading to activation of the membrane-bound photo-receptor. Data from solid-state ^{2}H NMR spectroscopy[21] and other biophysical measurements indicate the C13-methyl and the C=NH^{+}– moieties of the protonated Schiff base change their orientation upon ligand isomerization. The β-ionone ring with the C5-methyl group remains in its hydrophobic pocket, but its displacement due to elongation of retinal triggers allosteric movements of helices H5 and H6 that lead to rhodopsin activation (see text).
Figure produced with PyMOL [http://pymol.sourceforge.net/].

hydrogen bond between Glu122 and His211 may be responsible for rotation of the cytoplasmic end of the helix H5 towards to H6.[93] This motion destabilizes the ionic lock between helices H3 and H6 involving Glu134, Arg135, and Glu247 by bringing Tyr223 into close contact with the Arg135 residue, as indicated by Figure 17.10.

Consequently, the activating rotation of the helix H6 as first shown by Hubbell and co-workers[3,6] provides for a transient opening of the transducin (G_t) binding site.[11,12,21,95,113] New interactions between Tyr223–Arg135 and Glu247–Lys231–Thr251 are formed that stabilize the active Meta II conformation. Rhodopsin activation involves collective fluctuations of transmembrane helices (H5 and H6) in the Meta I–Meta II equilibrium. The reversible helix movements have large activation barriers; they occur infrequently due to their collective nature, because they involve displacements

of many atoms within the protein on the ms timescale. They match the catalytic turnover rate for G_t binding and activation by rhodopsin. An important role of collective helix fluctuations in activation of transducin in the photo-transduction cascade is suggested,[95] where a single photo-activated rhodopsin catalyzes the activation of hundreds of transducin molecules. Receptor activation is thus due to a fluctuating equilibrium among states and substates, which may be characteristic for other GPCRs in a membrane lipid environment.

17.6 Conclusions

Solid-state ^{2}H NMR spectroscopy gives a unique avenue for investigating G-protein-coupled receptors and other membrane proteins that is complementary to other biophysical approaches, such as X-ray crystallography. A distinct advantage of solid-state ^{2}H NMR spectroscopy is that rhodopsin is studied in a native-like membrane lipid environment.[114,115] Using ^{2}H NMR methods, the structure and dynamics of retinal have been investigated in the rhodopsin dark state, as well as in the Meta I and Meta II photointermediates. Despite its phenomenal stability in the dark state, the retinal cofactor of rhodopsin has significant dynamics within the binding pocket of the receptor. The ^{2}H NMR data indicate that the methyl groups are rapidly rotating. However, the off-axial motions are highly restricted in all the states of rhodopsin investigated (dark, Meta I, Meta II), with order parameters of ~ 0.9 due to interactions within the binding pocket. Solid-state ^{2}H NMR data combined with the results of other structural and biophysical studies suggest that displacement of the retinal β-ionone ring and rotation of the polyene chain occur upon photo-isomerization. Disruption of hydrogen bonding networks and ionic locks that stabilize the inactive conformation then lead to triggering of the activating helical fluctuations of the receptor. The Meta I–Meta II equilibrium of rhodopsin entails a complex energy landscape, with multiple substates rather than a simple on-off switch, with broad implications for biological signalling in general.

Acknowledgments

Research was supported in part by grants from the U.S. National Institutes of Health. Discussions with K. P. Hofmann, W. L. Hubbell, J. W. Lewis, G. F. J. Salgado, R. Vogel, and X. Xu are gratefully acknowledged.

References

1. D. M. Rosenbaum, S. G. F. Rasmussen and B. K. Kobilka, *Nature*, 2009, **459**, 356–363.
2. K. P. Hofmann, P. Scheerer, P. W. Hildebrand, H.-W. Choe, J. H. Park, M. Heck and O. P. Ernst, *Trends Biochem. Sci.*, 2009, **34**, 540–552.
3. D. L. Farrens, C. Altenbach, K. Yang, W. L. Hubbell and H. G. Khorana, *Science*, 1996, **274**, 768–770.

4. W. L. Hubbell, C. Altenbach, C. M. Hubbell and H. G. Khorana, *Adv. Protein Chem.*, 2003, **63**, 243–290.
5. B. Knierim, K. P. Hofmann, O. P. Ernst and W. L. Hubbell, *Proc. Natl. Acad. Sci. U. S. A.*, 2007, **104**, 20290–20295.
6. C. Altenbach, A. K. Kusnetzow, O. P. Ernst, K. P. Hofmann and W. L. Hubbell, *Proc. Natl. Acad. Sci. U. S. A.*, 2008, **105**, 7439–7444.
7. K. Palczewski, T. Kumasaka, T. Hori, C. A. Behnke, H. Motoshima, B. A. Fox, I. Le Trong, D. C. Teller, T. Okada, R. E. Stenkamp, M. Yamamoto and M. Miyano, *Science*, 2000, **289**, 739–745.
8. D. C. Teller, T. Okada, C. A. Behnke, K. Palczewski and R. E. Stenkamp, *Biochemistry*, 2001, **40**, 7761–7772.
9. T. Okada, Y. Fujiyoshi, M. Silow, J. Navarro, E. M. Landau and Y. Shichida, *Proc. Natl. Acad. Sci. U.S.A.*, 2002, **99**, 5982–5987.
10. T. Okada, M. Sugihara, A.-N. Bondar, M. Elstner, P. Entel and V. Buss, *J. Mol. Biol.*, 2004, **342**, 571–583.
11. H.-W. Choe, Y. J. Kim, J. H. Park, T. Morizumi, E. F. Pai, N. Krauß, K. P. Hofmann, P. Scheerer and O. P. Ernst, *Nature*, 2011, **471**, 651–656.
12. J. Standfuss, P. C. Edwards, A. D'Antona, M. Fransen, G. Xie, D. D. Oprian and G. F. X. Schertler, *Nature*, 2011, **471**, 656–660.
13. G. F. J. Salgado, A. V. Struts, K. Tanaka, N. Fujioka, K. Nakanishi and M. F. Brown, *Biochemistry*, 2004, **43**, 12819–12828.
14. P. J. R. Spooner, J. M. Sharples, M. A. Verhoeven, J. Lugtenberg, C. Glaubitz and A. Watts, *Biochemistry*, 2002, **41**, 7549–7555.
15. P. J. R. Spooner, J. M. Sharples, S. C. Goodall, H. Seedorf, M. A. Verhoeven, J. Lugtenburg, P. H. M. Bovee-Geurts, W. J. DeGrip and A. Watts, *Biochemistry*, 2003, **42**, 13371–13378.
16. P. J. R. Spooner, J. M. Sharples, S. C. Goodall, P. H. M. Bovee-Geurts, M. A. Verhoeven, J. Lugtenburg, A. M. A. Pistorius, W. J. DeGrip and A. Watts, *J. Mol. Biol.*, 2004, **343**, 719–730.
17. P. J. E. Verdegem, P. H. M. Bovee-Geurts, W. J. de Grip, J. Lugtenburg and H. J. M. de Groot, *Biochemistry*, 1999, **38**, 11316–11324.
18. A. B. Patel, E. Crocker, M. Eilers, A. Hirshfeld, M. Sheves and S. O. Smith, *Proc. Natl. Acad. Sci. U.S.A.*, 2004, **101**, 10048–10053.
19. E. Crocker, M. Eilers, S. Ahuja, V. Hornak, A. Hirshfeld, M. Sheves and S. O. Smith, *J. Mol. Biol.*, 2006, **357**, 163–172.
20. A. V. Struts, G. F. J. Salgado, K. Tanaka, S. Krane, K. Nakanishi and M. F. Brown, *J. Mol. Biol.*, 2007, **372**, 50–66.
21. A. V. Struts, G. F. J. Salgado and M. F. Brown, *Proc. Natl. Acad. Sci. U. S. A.*, 2011, **108**, 8263–8268.
22. S. H. Park, B. B. Das, F. Casagrande, Y. Tian, H. J. Nothnagel, M. Chu, H. Kiefer, K. Maier, A. A. De Angelis, F. M. Marassi and S. J. Opella, *Nature*, 2012, **491**, 779–783.
23. V. Cherezov, D. M. Rosenbaum, M. A. Hanson, S. G. F. Rasmussen, F. S. Thian, T. S. Kobilka, H.-J. Choi, P. Kuhn, W. I. Weis, B. K. Kobilka and R. C. Stevens, *Science*, 2007, **318**, 1258–1265.

24. S. G. F. Rasmussen, H.-J. Choi, D. M. Rosenbaum, T. S. Kobilka, F. S. Thian, P. C. Edwards, M. Burghammer, V. R. P. Ratnala, R. Sanishvili, R. F. Fischetti, G. F. X. Schertler, W. I. Weis and B. K. Kobilka, *Nature*, 2007, **450**, 383–387.
25. T. Warne, M. J. Serrano-Vega, J. G. Baker, R. Moukhametzianov, P. C. Edwards, R. Henderson, A. G. W. Leslie, C. G. Tate and G. F. X. Schertler, *Nature*, 2008, **454**, 486–491.
26. V.-P. Jaakola, M. T. Griffith, M. A. Hanson, V. Cherezov, E. Y. T. Chien, J. R. Lane, A. P. Ijzerman and R. C. Stevens, *Science*, 2008, **322**, 1211–1217.
27. A. Manglik, A. C. Kruse, T. S. Kobilka, F. S. Thian, J. M. Mathiesen, R. K. Sunahara, L. Pardo, B. K. Kobilka and S. Granier, *Nature*, 2012, **485**, 321–326.
28. S. Granier, A. Manglik, A. C. Kruse, T. S. Kobilka, F. S. Thian, W. I. Weis and B. K. Kobilka, *Nature*, 2012, **485**, 400–404.
29. H. Wu, D. Wacker, M. Mileni, V. Katritch, G. W. Han, E. Vardy, W. Liu, A. A. Thompson, X.-P. Huang, F. I. Carroll, S. W. Mascarella, R. B. Westkaemper, P. D. Mosier, B. L. Roth, V. Cherezov and R. C. Stevens, *Nature*, 2012, **485**, 327–332.
30. A. A. Thompson, W. Liu, E. Chung, V. Katritch, H. Wu, E. Vardy, X.-P. Huang, C. Trapella, R. Guerrini, G. Calo, B. L. Roth, V. Cherezov and R. C. Stevens, *Nature*, 2012, **485**, 395–399.
31. R. Nygaard, T. M. Frimurer, B. Holst, M. M. Rosenkilde and T. W. Schwartz, *Trends Pharmacol. Sci.*, 2009, **30**, 249–259.
32. S. Ahuja and S. O. Smith, *Trends Pharmacol. Sci.*, 2009, **30**, 494–502.
33. H. Nakamichi and T. Okada, *Angew. Chem. Int. Ed.*, 2006, **45**, 4270–4273.
34. D. Salom, D. T. Lodowski, R. E. Stenkamp, I. Le Trong, M. Golczak, B. Jastrzebska, T. Harris, J. A. Ballesteros and K. Palczewski, *Proc. Natl. Acad. Sci. U. S. A.*, 2006, **103**, 16123–16128.
35. X. Deupi, P. Edwards, A. Singhal, B. Nickle, D. Oprian, G. Schertler and J. Standfuss, *Proc. Natl. Acad. Sci. U. S. A.*, 2012, **109**, 119–124.
36. M. F. Brown, *Chem. Phys. Lipids*, 1994, **73**, 159–180.
37. A. V. Botelho, N. J. Gibson, Y. Wang, R. L. Thurmond and M. F. Brown, *Biochemistry*, 2002, **41**, 6354–6368.
38. A. V. Botelho, T. Huber, T. P. Sakmar and M. F. Brown, *Biophys. J.*, 2006, **91**, 4464–4477.
39. M. F. Brown, *Biochemistry*, 2012, **51**, 9782–9795.
40. P. Kukura, D. W. McCamant, S. Yoon, D. B. Wandschneider and R. A. Mathies, *Science*, 2005, **310**, 1006–1009.
41. T. P. Sakmar, S. T. Menon, E. P. Marin and E. S. Awad, *Annu. Rev. Biophys. Biomol. Struct.*, 2002, **31**, 443–484.
42. S. Lüdeke, R. Beck, E. C. Y. Yan, T. P. Sakmar, F. Siebert and R. Vogel, *J. Mol. Biol.*, 2005, **353**, 345–356.
43. K. Nakanishi and R. Crouch, *Isr. J. Chem.*, 1995, **35**, 253–272.
44. A. S. Ulrich, I. Wallat, M. P. Heyn and A. Watts, *Nat. Struct. Biol*, 1995, **2**, 190–192.

45. S. Moltke, A. A. Nevzorov, N. Sakai, I. Wallat, C. Job, K. Nakanishi, M. P. Heyn and M. F. Brown, *Biochemistry*, 1998, **37**, 11821–11835.
46. S. Moltke, I. Wallat, N. Sakai, K. Nakanishi, M. F. Brown and M. P. Heyn, *Biochemistry*, 1999, **38**, 11762–11772.
47. G. F. J. Salgado, A. V. Struts, K. Tanaka, S. Krane, K. Nakanishi and M. F. Brown, *J. Am. Chem. Soc.*, 2006, **128**, 11067–11071.
48. M. Etzkorn, S. Martell, O. C. Andronesi, K. Seidel, M. Engelhard and M. Baldus, *Angew. Chem. Int. Ed.*, 2007, **46**, 459–462.
49. K. Varga, L. Tian and A. E. McDermott, *Biochim. Biophys. Acta*, 2007, **1774**, 1604–1613.
50. A. Watts, *Nat. Rev. Drug Discovery*, 2005, **4**, 555–568.
51. M. F. Brown, K. Martínez-Mayorga, K. Nakanishi, G. F. J. Salgado and A. V. Struts, *Photochem. Photobiol.*, 2009, **85**, 442–453.
52. V. Copié, A. E. McDermott, K. Beshah, J. C. Williams, M. Spyker-Assink, R. T. Gebhard, J. Lugtenberg, J. Herzfeld and R. G. Griffin, *Biochemistry*, 1994, **33**, 3280–3286.
53. A. A. Nevzorov and S. J. Opella, *J. Magn. Reson.*, 2003, **160**, 33–39.
54. S. Ahuja, V. Hornak, E. C. Y. Yan, N. Syrett, J. A. Goncalves, A. Hirshfeld, M. Ziliox, T. P. Sakmar, M. Sheves, P. J. Reeves, S. O. Smith and M. Eilers, *Nat. Struct. Mol. Biol.*, 2009, **16**, 168–175.
55. F. Hu, W. Luo and M. Hong, *Science*, 2010, **330**, 505–508.
56. M. Hong, Y. Zhang and F. Hu, *Annu. Rev. Phys. Chem.*, 2012, **63**, 1–24.
57. A. E. McDermott, *Curr. Opin. Struct. Biol.*, 2004, **14**, 554–561.
58. A. E. McDermott, *Annu. Rev. Biophys.*, 2009, **38**, 385–403.
59. T. A. Cross, M. Sharma, M. Yi and H.-X. Zhou, *Trends Biochem. Sci.*, 2011, **36**, 117–125.
60. M. Sharma, M. Yi, H. Dong, H. Qin, E. Peterson, D. D. Busath, H.-X. Zhou and T. A. Cross, *Science*, 2010, **330**, 509–512.
61. M. F. Brown, in *Biological Membranes. A Molecular Perspective from Computation and Experiment*, ed. K. Merz Jr. and B. Roux, Birkhäuser, Basel, 1996, pp. 175–252.
62. A. A. Nevzorov, S. Moltke, M. P. Heyn and M. F. Brown, *J. Am. Chem. Soc.*, 1999, **121**, 7636–7643.
63. A. Kusumi and J. S. Hyde, *Biochemistry*, 1982, **21**, 5978–5983.
64. M. F. Brown and S. I. Chan, in *Encyclopedia of Nuclear Magnetic Resonance*, ed. D. M. Grant and R. K. Harris, Wiley, New York, 1996, vol. 2 , pp. 871–885.
65. K. Schmidt-Rohr and H. W. Spiess, *Multidimensional Solid State NMR and Polymers*, Academic Press, San Diego, 1994.
66. C. P. Slichter, *Principles of Magnetic Resonance*, Springer, Heidelberg, 3rd edn, 1990.
67. A. A. Nevzorov, S. Moltke and M. F. Brown, *J. Am. Chem. Soc.*, 1998, **120**, 4798–4805.
68. T. Huber, A. V. Botelho, K. Beyer and M. F. Brown, *Biophys. J.*, 2004, **86**, 2078–2100.
69. M. Chabre and J. Breton, *Vision Res.*, 1979, **19**, 1005–1018.

70. M. Michel-Villaz, C. Roche and M. Chabre, *Biophys. J.*, 1982, **37**, 603–616.
71. J. W. Lewis, C. M. Einterz, S. J. Hug and D. S. Kliger, *Biophys. J.*, 1989, **56**, 1101–1111.
72. S. Jäger, J. W. Lewis, T. A. Zvyaga, I. Szundi, T. P. Sakmar and D. S. Kliger, *Proc. Natl. Acad. Sci. U. S. A.*, 1997, **94**, 8557–8562.
73. Y. Fujimoto, J. Ishihara, S. Maki, N. Fujioka, T. Wang, T. Furuta, N. Fishkin, B. Borhan, N. Berova and K. Nakanishi, *Chem. Eur. J.*, 2001, **7**, 4198–4204.
74. Y. Fujimoto, N. Fishkin, G. Pescitelli, J. Decatur, N. Berova and K. Nakanishi, *J. Am. Chem. Soc.*, 2002, **124**, 7294–7302.
75. J. Cavanaugh, W. J. Fairbrother, A. G. Palmer III, N. J. Skelton and M. Rance, *Protein NMR Spectroscopy: Principles and Practice*, Academic Press, New York, 2nd edn, 2006.
76. N. Fishkin, N. Berova and K. Nakanishi, *Chem. Rec.*, 2004, **4**, 120–135.
77. S. O. Smith, I. Palings, M. E. Miley, J. Courtin, H. de Groot, J. Lugtenberg, R. A. Mathies and R. G. Griffin, *Biochemistry*, 1990, **29**, 8158–8164.
78. G. S. Harbison, S. O. Smith, J. A. Pardoen, J. M. L. Courtin, J. Lugtenburg, J. Herzfeld, R. A. Mathies and R. G. Griffin, *Biochemistry*, 1985, **24**, 6955–6962.
79. B. Mertz, M. Lu, M. F. Brown and S. E. Feller, *Biophys. J.*, 2011, **101**, L18–L19.
80. S. Zhu, M. F. Brown and S. E. Feller, *J. Am. Chem. Soc.*, 2013, **135**, 9391–9398.
81. P.-W. Lau, A. Grossfield, S. E. Feller, M. C. Pitman and M. F. Brown, *J. Mol. Biol.*, 2007, **372**, 906–917.
82. N. Leioatts, B. Mertz, K. Martínez-Mayorga, T. D. Romo, M. C. Pitman, S. E. Feller, A. Grossfield and M. F. Brown, *Biochemistry*, 2014 in press.
83. G. Gröbner, I. J. Burnett, C. Glaubitz, G. Choi, A. J. Mason and A. Watts, *Nature*, 2000, **405**, 810–813.
84. G.-F. Jang, V. Kuksa, S. Filipek, F. Bartl, E. Ritter, M. H. Gelb, K. P. Hofmann and K. Palczewski, *J. Biol. Chem.*, 2001, **276**, 26148–26153.
85. Q. Wang, R. W. Schoenlein, L. A. Peteanu, R. A. Mathies and C. V. Shank, *Science*, 1994, **266**, 422–424.
86. S. W. Lin, M. Groesbeek, I. van der Hoef, P. Verdegem, J. Lugtenburg and R. A. Mathies, *J. Phys. Chem. B*, 1998, **102**, 2787–2806.
87. T. Andruniów, N. Ferré and M. Olivucci, *Proc. Natl. Acad. Sci. U. S. A.*, 2004, **101**, 17908–17913.
88. D. Polli, P. Altoè, O. Weingart, K. M. Spillane, C. Manzoni, D. Brida, G. Tomasello, G. Orlandi, P. Kukura, R. A. Mathies, M. Garavelli and G. Cerullo, *Nature*, 2010, **467**, 440–443.
89. J. A. Gascon and V. S. Batista, *Biophys. J.*, 2004, **87**, 2931–2941.

90. M. Sugihara, J. Hufen and V. Buss, *Biochemistry*, 2006, **45**, 801–810.
91. S. Hayashi, E. Tajkhorshid and K. Schulten, *Biophys. J.*, 2009, **96**, 403–416.
92. J. J. Ruprecht, T. Mielke, R. Vogel, C. Villa and G. F. X. Schertler, *EMBO J.*, 2004, **23**, 3609–3620.
93. S. Ahuja, E. Crocker, M. Eilers, V. Hornak, A. Hirshfeld, M. Ziliox, N. Syrett, P. J. Reeves, H. G. Khorana, M. Sheves and S. O. Smith, *J. Biol. Chem.*, 2009, **284**, 10190–10201.
94. R. Vogel, F. Siebert, S. Lüdeke, A. Hirshfeld and M. Sheves, *Biochemistry*, 2005, **44**, 11684–11699.
95. A. V. Struts, G. F. J. Salgado, K. Martínez-Mayorga and M. F. Brown, *Nat. Struct. Mol. Biol.*, 2011, **18**, 392–394.
96. K. Martínez-Mayorga, M. C. Pitman, A. Grossfield, S. E. Feller and M. F. Brown, *J. Am. Chem. Soc.*, 2006, **128**, 16502–16503.
97. M. F. Brown, *J. Chem. Phys.*, 1982, **77**, 1576–1599.
98. T. P. Trouard, T. M. Alam and M. F. Brown, *J. Chem. Phys.*, 1994, **101**, 5229–5261.
99. D. A. Torchia and A. Szabo, *J. Magn. Reson.*, 1982, **49**, 107–121.
100. E. Meirovitch, Y. E. Shapiro, A. Polimeno and J. H. Freed, *Prog. Nucl. Magn. Reson. Spectrosc.*, 2010, **56**, 360–405.
101. E. Meirovitch, A. Polimeno and J. H. Freed, *J. Chem. Phys.*, 2010, **132**, 207101-1–207101-2.
102. E. Meirovitch, A. Polimeno and J. H. Freed, *J. Phys. Chem. B*, 2006, **110**, 20615–20628.
103. B. Halle, *J. Phys. Chem.*, 1991, **95**, 6724–6733.
104. L. S. Batchelder, C. H. Niu and D. A. Torchia, *J. Am. Chem. Soc.*, 1983, **105**, 2228–2231.
105. P. L. Nordio and P. Busolin, *J. Chem. Phys.*, 1971, **55**, 5485–5490.
106. P. L. Nordio, G. Rigatti and U. Segre, *J. Chem. Phys.*, 1972, **56**, 2117–2123.
107. A. A. Nevzorov and M. F. Brown, *J. Chem. Phys.*, 1997, **107**, 10288–10310.
108. A. Szabo, *J. Chem. Phys.*, 1984, **81**, 150–167.
109. A. A. Nevzorov, T. P. Trouard and M. F. Brown, *Phys. Rev. E*, 1998, **58**, 2259–2281.
110. R. Vogel, S. Lüdeke, F. Siebert, T. P. Sakmar, A. Hirshfeld and M. Sheves, *Biochemistry*, 2006, **45**, 1640–1652.
111. T. Okada, O. P. Ernst, K. Palczewski and K. P. Hofmann, *Trends Biochem. Sci.*, 2001, **26**, 318–324.
112. M. Mahalingam, K. Martínez-Mayorga, M. F. Brown and R. Vogel, *Proc. Natl. Acad. Sci. U. S. A.*, 2008, **105**, 17795–17800.
113. P. Scheerer, J. H. Park, P. W. Hildebrand, Y. J. Kim, N. Krauß, H.-W. Choe, K. P. Hofmann and O. P. Ernst, *Nature*, 2008, **455**, 497–502.
114. M. F. Brown, G. F. J. Salgado and A. V. Struts, *Biochim. Biophys. Acta*, 2010, **1798**, 177–193.

115. B. Mertz, A. V. Struts, S. E. Feller and M. F. Brown, *Biochim. Biophys. Acta*, 2012, **1818**, 241–251.
116. M. F. Brown, M. P. Heyn, C. Job, S. Kim, S. Moltke, K. Nakanishi, A. A. Nevzorov, A. V. Struts, G. F. J. Salgado and I. Wallat, *Biochim. Biophys. Acta*, 2007, **1768**, 2979–3000.
117. M. F. Brown and A. V. Struts, in *Encyclopedia of Biophysics*, ed. G. C. K. Roberts, Springer, Berlin, 2013, pp. 2231–2243.